CONTINUOUS PYROLYSIS OF CANMET RESIDUE IN ARGON/HYDROGEN PLASMA

by

Muftah Hassan El-Naas

Department of Chemical Engineering
McGill University

A Thesis Submitted to the Faculty of Graduate Studies
and Research in Partial Fulfillment of the
Requirements for the Degree of
Master of Engineering

March 1991


بسم الله الرحمن الرحيم

CONTINUOUS PYROLYSIS OF CANMET RESIDUE IN ARGON/HYDROGEN PLASMA

ABSTRACT

A laboratory-scale reactor with a feeding system was specially designed and built to study the continuous pyrolysis of CANMET coprocessing residue in Argon/Hydrogen plasma using an induction plasma torch. Hydrogen was injected into the argon plasma tailflame ranging in molar concentration from 0 to 23%. The residue was continuously fed to the reactor in liquid form at flow rates ranging from 6 to 9 g/min. The mean plasma temperature was varied from 2700 to 3670 K.

A maximum of 10% of the residue pyrolysed with up to 90% conversion to gaseous hydrocarbons. The rate of residue pyrolysis and the rate of formation of the gaseous products were found to be strongly dependent on heat transfer. The only gaseous products detected were acetylene, ethylene and methane. A considerable amount of soot was also observed, but no liquid hydrocarbons were produced. The soot contained some residue particles which were ejected into the gas phase in the form of small droplets during the pyrolysis. Due to the short gas residence time, these tiny particles reacted only to a small extent while entrained in the gas.

Elemental analysis of the unreacted residue, at the various operating conditions, showed that there was no change from the original, untreated CANMET residue. This indicated that the pyrolysis was uniform at those conditions and that there was no preferential removal of carbon, hydrogen or nitrogen.

RESUME

Un réacteur de laboratoire a été spécialement construit avec un système d'alimentation pour étudier la pyrolise du résidu du co-procédé CANMET dans un plasma d'argon et d'hydrogène grâce à une torche à induction. L'hydrogène était injectée dans la queue du plasma d'argon à des concentrations molaires de moins de 23 p.cent. Le résidu était introduit sous forme liquide, d'une manière continue dans le réacteur à des débits de 6 à 9 grammes par minutes. La température moyenne du plasma variait entre 2700 à 3670 K.

Un maximum de 10 p.cent du résidu a été pyrolisé, se convertissant à plus de 90 p.cent en hydrocarbures sous forme gazeuse. Les taux de pyrolise du résidu et de formation de produits gazeux sont fortement corrélés au transfert de chaleur. L'acétylène, l'éthylène et le méthane ont été les seuls produits gazeux détectés. Une grande quantité de suie a été observée, mais pas d'hydrocarbures liquide. La suie contenait des particules communes au résidu qui était projetées dans le gaz sous forme de petites gouttelettes durant la pyrolise. Ces petites particules n'ont que très peu réagit alors qu'elles étaient entrainées dans le gaz.

L'analyse des éléments du résidu n'ayant pas réagit a montré que le résidu original du procédé CANMET ne subissait aucune modification, peu importe les conditions d'opérations. C'est une indication que la pirolyse était uniforme sous ces conditions et qu'il n'y avait pas de mode préférentiel de suppression du carbone, de l'hydrogène ou de l'azote.

To My Mother,

Ghazala Ebraydan,

and in Loving Memory of My Father,

Hassan El-Naas

ACKNOWLEDGEMENTS

I would like to express my utmost appreciation and gratitude to those who contributed directly or indirectly to the completion of this work for their help and support. To them all, I say thanks.

First, I wish to thank my supervisors Dr. Richard Munz and Dr. Dimitrios Berk for their invaluable guidance and ever present enthusiasm. I would also like to thank my fellow graduate students and friends in the plasma group, especially, Chico Moura for the useful suggestions and discussions. I owe special thanks to Daphne Maravei for assisting with some of the experiments.

I would like to express my thanks to the staff of the Chemical Engineering Workshop: Mr. Krish, Allen Gagnon, Charles Dolan and, especially, Walter Greenland for doing a superb job in constructing the reactor and the feeding system. I am thankful to the Department of Chemical Engineering technicians: Mr. E. Siliauskas, N. Habib and L. Cusmich for their help and courtesy. I am also thankful to Mr. Jean Dumont of the Chemical Engineering Purchasing and Stores for making it easier to find whatever is needed.

Finally, I am deeply grateful for the help and encouragement that my family, especially, my brother Awad has always given to me.

TABLE OF CONTENTS

ABSTRACT i
RESUME ii
ACKNOWLEDGEMENTS iv
TABLE OF CONTENTS v
LIST OF FIGURES viii
LIST OF TABLES xii

INTRODUCTION 1

LITERATURE REVIEW 6
2.1 PLASMA 7
2.1.1 Plasma Generators 8
2.1.2 Plasma Processes 8

2.2 PLASMA PYROLYSIS OF FOSSIL FUELS 9
2.2.1 Plasma Reactions 9
2.2.2 Formation of Carbon Black 11
2.2.3 Formation of Liquid Hydrocarbons 12

APPARATUS AND PROCEDURE 13

3.1 APPARATUS 14
3.1.1 Power Supply and Plasma Torch 14
3.1.2 Reactor and Feeding System 16
3.1.3 Sampling Probe 19

3.2 EXPERIMENTAL PROCEDURE 19

ANALYTICAL TECHNIQUES 21

4.1 PRODUCT GAS 22

4.2 ELEMENTAL ANALYSIS 23

4.3 PLASMA TEMPERATURE 26

ANALYSIS OF THE RESIDUE 28

RESULTS AND DISCUSSION 32

6.1 EFFECT OF PLASMA GAS COMPOSITION 33
6.1.1 Achievement of Steady State 34
6.1.2 Effect of Sampling Location 36
6.1.3 Effect of Hydrogen Addition on Heat Transfer 38
6.1.4 Yield of Gaseous Hydrocarbons 44
6.1.5 Deposition of Soot 47

6.2 EFFECT OF PLASMA TEMPERATURE 49

6.3 EFFECT OF RESIDUE FLOW RATE 54

6.4 ISOLATION OF LIQUID HYDROCARBONS 57

6.5 ANALYSIS OF UNREACTED RESIDUE 58

6.6 THERMODYNAMIC ANALYSIS 58
6.6.1 Plasma Temperature 61
6.6.2 Plasma Gas Composition 64
6.6.3 Production of CO, HCN and H_2S 67
6.6.4 Effect of Including Graphite as a Solid Phase 70
6.6.5 Comparison with Experimental Results 71

6.7 COMPLETE CONVERSION 77

CONCLUSIONS 80

REFERENCES 84

APPENDICES 87

LIST OF FIGURES

Figure		Page
1.1	Schematic Flow Diagram of the CANMET Process.	4
3.1	Schematic Diagram of the Experimental Apparatus.	15
3.2	Cross-Sectional View of the Reactor.	18
4.1	Variation of Peak Area of Apparent Hydrogen with the Volume of the Sample Injected.	24
4.2	Variation of the Mean Plasma Temperature with Power Input.	27
6.1	Variation of Acetylene Concentration in the product gas with Time.	35
6.2	Variation of the Concentration of the Gaseous Hydrocarbons in the product gas with Sampling Position.	37
6.3	Calculated Plasma Temperature as a Function of Plasma Gas Composition.	40
6.4	Calculated Heat Transfer as a Function of Plasma gas Composition.	41

6.5	Effect of Plasma Gas Composition on Residue Conversion.	42
6.6	Effect of Plasma Gas Composition on Acetylene Concentration in the Product Gas.	43
6.7	Effect of Plasma Gas Composition on the Yield of Hydrocarbons.	46
6.8	Effect of Plasma Temperature on Residue Conversion.	51
6.9	Effect of Plasma Temperature on the Yield of Hydrocarbons.	52
6.10	Effect of Plasma Temperature on the Concentration of Gaseous Hydrocarbons.	53
6.11	Effect of Residue Flow Rate on Residue Conversion.	55
6.12	Effect of Residue Flow Rate on Acetylene Concentration in the Product Gas.	56
6.13	Variation of the C-H-N Content of the unreacted residue with Plasma Gas Composition.	59
6.14	Variation of the Predicted Equilibrium Composition with Plasma Temperature.	63
6.15	Variation of the Predicted Equilibrium Composition with Plasma Gas Composition.	65

6.16	Variation of the Predicted Equilibrium Concentration of CO and HCN with Plasma Temperature.	68
6.17	Variation of the Predicted Equilibrium Concentration of CO and HCN with Plasma Gas Composition.	69
6.18	Predicted Yield of Hydrocarbons as a Function of Plasma Gas Composition.	72
6.19	Predicted Yield of Hydrocarbons as a Function of Plasma Temperature.	73
6.20	Predicted and Experimental Yield of Hydrocarbons as a Function of Plasma Temperature.	75
6.21	Predicted and Experimental Yield of Hydrocarbons as a Function of Plasma Gas Composition.	76
6.22	Variation of Crucible Temperature with Power Input.	79
	Appendix A: Calibration curves for the various gases used to calibrate the gas chromatograph.	
A.1	Calibration for Argon.	89
A.2	Calibration for Hydrogen.	90
A.3	Calibration for Acetylene.	91
A.4	Calibration for Ethylene.	92

A.5	Calibration for Methane.	93
A.6	Calibration for Nitrogen.	94
A.7	Calibration for Carbon Dioxide.	95
A.8	Calibration for Carbon Monoxide.	96

LIST OF TABLES

Table		Page
5.1	Elemental Analysis of the CANMET Residue.	30
6.1	Elemental Analysis of Soot and the CANMET Residue.	49
6.2	Conditions for Thermodynamic Calculations of Equilibrium Composition as a Function of Plasma Temperature.	62
6.3	Conditions for Thermodynamic Calculations of Equilibrium Composition as a Function of Plasma Gas Composition.	66
C.1	Heat Capacity at Constant Pressure for Carbon, Hydrogen, Nitrogen, Sulphur and Oxygen Containing Compounds for the Temperature Range 298 to 2000 K.	102
C.2	Heat Capacity at Constant Pressure for Carbon, Hydrogen, Nitrogen, Sulphur and Oxygen Containing Compounds for the Temperature Range 2000 to 6000 K.	104

- 1 -

INTRODUCTION

Upgrading of heavy oil to light liquid hydrocarbons has attracted a great deal of attention in the past few years. This attention is mainly due to the pressing need for an energy source that may replace the conventional oil reserves that are being gradually depleted. Compared to conventional light crude, heavy oil has lower hydrogen-to-carbon ratio and has higher levels of sulphur, nitrogen and metals. It is this high level of contaminants that causes the major difficulty in upgrading. The primary objective of upgrading is to convert heavy oil to transportable products that can be processed in conventional refineries. Upgrading can be achieved either through the removal of carbon (cracking), the addition of hydrogen (hydrogenation) or both. Numerous upgrading commercial processes are available. A review of a few upgrading processes was given by Schumacher (1982).

A process for heavy oil upgrading and coal liquification has been developed by CANMET (Canada Center for Mineral and Energy Technology). The process involves simultaneous upgrading of coal and heavy oil, and therefore it is usually referred to as coprocessing. An additive, made of fine coal particles impregnated with iron sulphate or other metallic salts (acting as a catalyst), is mixed with heavy oil and hydrogenated at high temperature in an upflow tubular reactor. The additive, which usually represents 0.5 to 5 wt% of the feed, allows operation at reduced pressure relative to other competitive processes and suppresses coke formation (Menzies et al, 1981). Other features of the CANMET process include high

conversion and high overall liquid and light distillate yield. The products of hydrogenation are flashed to separate lighter and heavier components. Light gases are passed through scrubbers to remove toxic by-products while heavier components are separated by distillation to obtain a distillate and a residue; a flow diagram of the process is shown in Figure 1.1.

The residue, which is solid at room temperature, contains the added metallic salt (catalyst) and most of the metals present in the oil. It is the utilization of this residue that represents a major challenge to the CANMET process. Disposing of the residue could result in economical and environmental problems. The high level of contaminants in the residue poses a major hazard to the environment. Moreover, if a more active and a more expensive catalyst were to be used, loss of such catalyst with the residue would elevate the operating costs of the process.

Plasma processing is being considered as a possible method for treating the CANMET coprocessing residue. The aim of such a treatment would be to recover the catalyst in a useful form and, at the same time, produce some commercially attractive products such as acetylene, ethylene and some liquid hydrocarbons. CANMET is considering the co-current pyrolysis of atomized liquid residue in hydrogen plasma. This would involve the reaction of falling micro-droplets with hydrogen at high temperature. Treatment of the residue in a single particle batch reactor was studied by Dlugogorski (1989). His objective was to study the

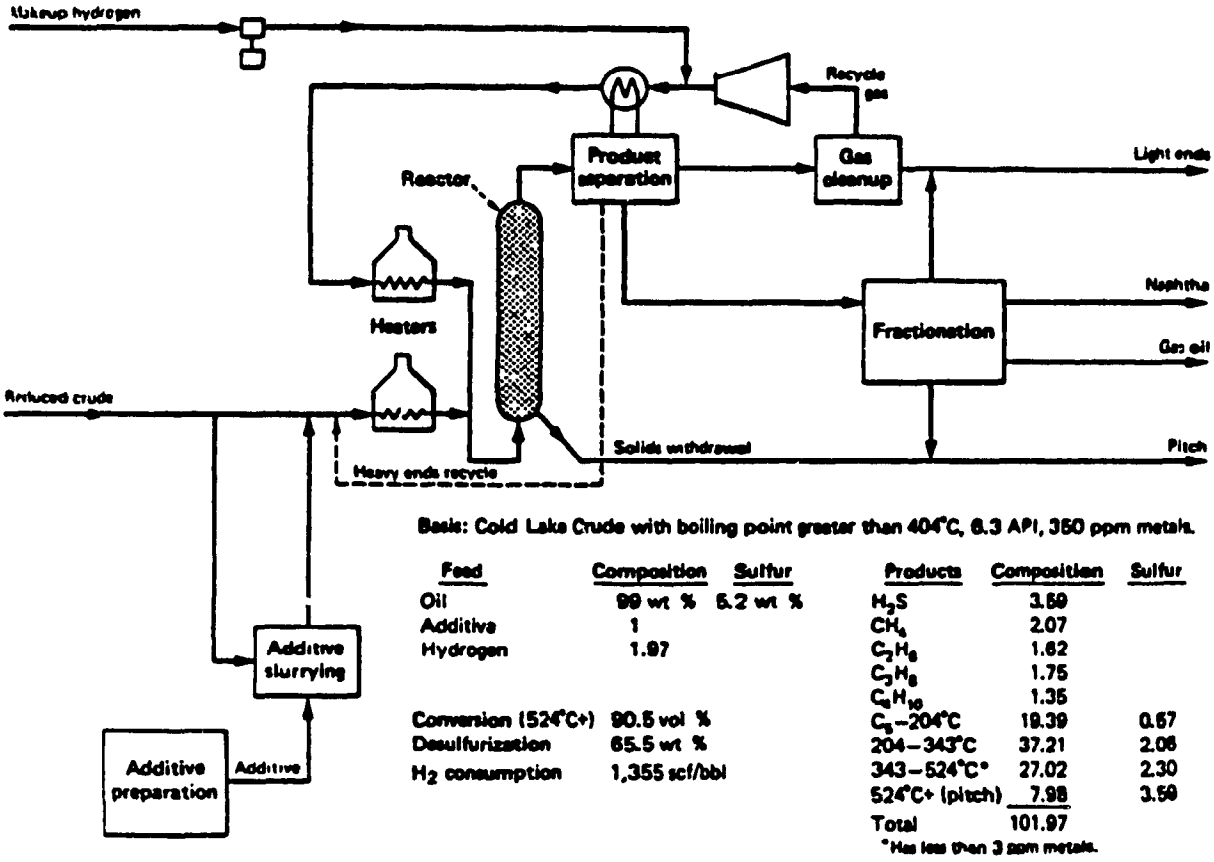

Basis: Cold Lake Crude with boiling point greater than 404°C, 6.3 API, 350 ppm metals.

Feed	Composition	Sulfur
Oil	99 wt %	5.2 wt %
Additive	1	
Hydrogen	1.97	
Conversion (524°C+)	90.5 vol %	
Desulfurization	65.5 wt %	
H_2 consumption	1,355 scf/bbl	

Products	Composition	Sulfur
H_2S	3.59	
CH_4	2.07	
C_2H_6	1.62	
C_3H_8	1.75	
C_4H_{10}	1.35	
C_5–204°C	19.39	0.67
204–343°C	37.21	2.06
343–524°C*	27.02	2.30
524°C+ (pitch)	7.98	3.59
Total	101.97	

*Has less than 3 ppm metals.

Figure 1.1

Schematic Flow Diagram of the CANMET Process.

(Menzies et al, 1981)

pyrolysis of the residue in argon/hydrogen plasma under different operating conditions.

Due to the transient nature of batch reactors, it is not possible to reach steady state, and therefore one can not study the reactions and the controlling mechanisms involved. Thus, the main objective of the present work was to study the continuous pyrolysis of the residue in argon/hydrogen plasma under different operating conditions of plasma temperature, plasma gas composition and residue flow rate. A laboratory-scale reactor with a feeding system was specially designed and built to study the pyrolysis using an induction plasma torch. The effect of the various operating conditions on the composition of the gaseous products, the rate of residue pyrolysis and the state of the residue after treatment was investigated.

The rest of this thesis is divided into six chapters. The second chapter is a review of previous work on plasma and plasma pyrolysis. The third chapter gives a description of the experimental apparatus and procedure. Analytical techniques and analysis of the CANMET coprocessing residue are given in the forth and fifth chapter, respectively. The sixth chapter contains the experimental results and discussion. Finally, the conclusions are given in the seventh chapter.

- 2 -

LITERATURE REVIEW

2.1 PLASMA

The history of plasma can be traced back to the early studies of discharge in gases associated with such names as those of Michael Faraday and William Crookes. In 1879, Crookes noticed that gases under electric discharge (ionized gases) possessed unusual physical and chemical properties. This led him to suggest that those gases can be regarded as a fourth state of matter (McTaggart, 1967). In 1928, Langmuir was the first to use the word "plasma" to denote ionized gases.

Plasma is now known as an ionized gas containing molecules, atoms, ions, electrons and photons (Fauchais et al., 1987). The negative and positive charges in plasma are approximately equal making it neutral overall. Plasma can be divided into two different types: thermal or equilibrium plasma and non-thermal or non-equilibrium plasma. In thermal plasmas, the electron temperature is approximately equal to the temperature of the heavy particles. In non-thermal plasmas, the heavy particles temperature is much lower than that of the electron. In some literature these two types are referred to as hot and cold plasmas respectively. The hot or thermal plasmas are formed at atmospheric or higher pressures. Plasmas produced in spray torches, radio frequency inductive torches, and electric arcs are typical examples of hot plasmas. Cold plasmas are formed under reduced pressure; examples of this type include plasmas produced in glow discharges and in corona discharges.

2.1.1 Plasma Generators

Plasma may be generated by applying a high frequency high voltage electric field to a gas. Plasma generating devices can be classified as having electrodes or being electrodeless. Electrode devices (sometimes called thermal or plasma arcs) are characterized by the presence of a cathode and an anode. Transferred arcs and non-transferred arcs are the only two types of thermal arcs. Further details about electrode devices can be found in the works of Mehmetoglu (1980) and Patterson (1983).

Electrodeless devices, as the name implies, do not have electrodes; thus the plasma is initiated either by capacitive or inductive coupling. A high frequency electric field is used to maintain the discharge in capacitive coupling, whereas in inductive coupling, the discharge is maintained by a time-varying magnetic field. For more details about these devices, readers are referred to the work of Munz (1974), Sayegh (1977), Biceroglu (1978) and Pfender et al.(1987).

2.1.2 Plasma Processes

Plasmas have been applied to mechanical processes such as welding, cutting and spraying; metallurgical processes such as the production of alloys and the making of refractory materials; and chemical processes such as the synthesis of acetylene,

nitrogen oxides and phosphates as well as the production of new ceramics (Labort et al, 1981). Plasma processes have several advantages over traditional processes. The high energy associated with plasma results in faster reactions and faster physical transformations and therefore more output using smaller equipment. This also allows the possibility of making new products such as high temperature ultra fine ceramics. Moreover, the use of electrical energy for heating allows separation of process energy and chemistry.

2.2 PLASMA PYROLYSIS OF FOSSIL FUELS

Over the past forty years, there has been an extensive amount of research on the processing of fossil fuels using hydrogen, steam and other kinds of plasmas. Venugopalan and co-workers (1980) gave a detailed review of the plasma chemistry of fossil fuels. A more recent and thorough literature review of fossil fuel plasmas was given by Dlugogorski (1989). Only the work that is closely related to this thesis will be reviewed here.

2.2.1 Plasma Reactions

The pyrolysis of hydrocarbons in hydrogen plasma was studied by Gehrmann and Schmidt (1971). They found that gas residence time was critical in determining the major product. A residence time greater than 4 ms resulted in a reduction of

acetylene formation and favoured the formation of methane. Also, very small residence time (less than 1 ms) reduced the production of acetylene and ethylene.

Baumann et al (1988) studied the pyrolysis of coal in hydrogen and helium plasma. The study showed that the yield of acetylene, as the major product, was governed by fast reactions between coal primary volatiles and highly reactive plasma species. It was also found that coal pyrolysis was strongly dependent on heat transfer and independent of plasma medium. A study of the gas phase reaction of coal volatiles in hydrogen plasma was conducted by Beiers et al (1988). They used liquid and gaseous hydrocarbons to simulate the reaction of coal volatiles at atmospheric pressures and temperatures from 1273 to 2273 K. They found that hydrocarbons reacted rapidly with plasma species (H atoms, excited atoms, molecules and ions). The researchers suggested that these fast reactions did not reach thermodynamic equilibrium, and therefore they were expected to be followed by slow reactions that could not be observed due to short residence time. This led them to conclude that plasma pyrolysis was different from conventional pyrolysis and could not be described by 'conventional kinetic pyrolysis data'.

The treatment of CANMET coprocessing residue in a single particle semi-batch reactor in argon and argon/hydrogen plasma was studied by Dlugogorski (1989). He reported that up to 50% of the treated residue reacted to form acetylene, methane, ethylene, carbon monoxide, and soot. Hydrogen and oxygen in the organic part of

the residue were preferentially removed, while nitrogen and sulphur were retained in the unconverted residue. The low conversion was attributed to the low pyrolysis temperature. Due to cooling by radiation, the sample-containing crucible had much lower temperature than that of the plasma. The study also showed that carbon conversion to gaseous hydrocarbons increased to 24% with hydrogen addition compared to 14% achieved with pure argon plasma. Hydrogen was injected into the argon plasma tailflame. The effect of injecting more than 10% (mol) hydrogen into the plasma tailflame on the conversion was negligible.

2.2.2 Formation of Carbon Black

Carbon black is a by-product resulting from the decomposition of acetylene in most processes involving reactions of hydrocarbons. Spangenberg (1981) showed that if a reaction involving hydrocarbons was not quenched rapidly, acetylene would decompose in a chain reaction to form soot (carbon black). The formation of carbon black during cracking of hydrocarbons in hydrogen plasma was studied by Bolouri and Amouroux (1983). They found that operating conditions, especially temperature, play an important role in the precipitation of carbon. They noted that at temperatures higher than 3000 K, molecular carbon and radicals (C, C_2, C_3, H, and C_2H) were predominant. Thus, molecular carbon precipitates as carbon black; however, if this mixture is quenched, C_2H will react with H to form acetylene (Plooster and Reed, 1959).

2.2.3 Formation of Liquid Hydrocarbons

Baronnet et al (1987) studied the pyrolysis of paraffins and high molecular weight hydrocarbons in hydrogen/methane plasma. They found that conversion to liquid hydrocarbons depended mainly on molecular structure. High molecular weight cycloalkanes and aromatics had conversions to liquid hydrocarbons of 12%, while long chain paraffins had only 2% conversion.

A recent study of hydropyrolysis of heavy oil showed that formation of liquid hydrocarbons was mostly influenced by reaction temperature (Hikita et al, 1989). In the study, four kinds of heavy oils (Orinco tar, Arabian vacuum residue, coal tar and Minas vacuum residue) were hydropyrolysed at temperatures ranging from 773 to 1273 K. It was found that at temperature below 973 K, benzene was stable and could be a major product. Higher temperatures, however, increased the conversion to gas and decreased that to liquids regardless of oil type. Although the study was conducted for long residence times (15 to 60 s), the researchers found that the effect of reaction temperature was far more important than that of residence time. Thus, the formation of liquid hydrocarbons can be influenced both by the molecular structure of the hydrocarbon and the reaction temperature.

- 3 -

APPARATUS AND PROCEDURE

3.1 APPARATUS

The experimental set-up consisted of a high frequency power supply, an induction plasma torch, a reactor with continuous feeding system and a sampling system. With the exception of the feeding system, all components of the apparatus were water cooled. A schematic diagram of the apparatus is shown in Figure 3.1.

3.1.1 Power Supply and Plasma Torch

The power supply was a radio frequency oscillator manufactured by Lepel High Frequency Laboratories Inc. as a Model TAFA-32*30 MC. It takes a power input of three phase 60 Hz and transforms it into a maximum 30 kW at 4 MHz. The unit was controlled so as to prevent operation at low cooling water pressure (less than 515 kPa) or low plasma gas pressure (less than 377 kPa).

The radio frequency induction plasma torch was a TAFA Model 56. It consisted of a quartz tube with 38 mm internal diameter and 3 mm thickness. The tube was surrounded by an induction coil which was immersed in cooling water. When current is passed through the coil, it induces a time varying magnetic field which in turn induces an electric field inside the tube. The tube was internally coated with gold to facilitate ignition of the plasma. Argon was used to initiate and sustain the plasma, and it was injected tangentially and axially through a gas distributor on top

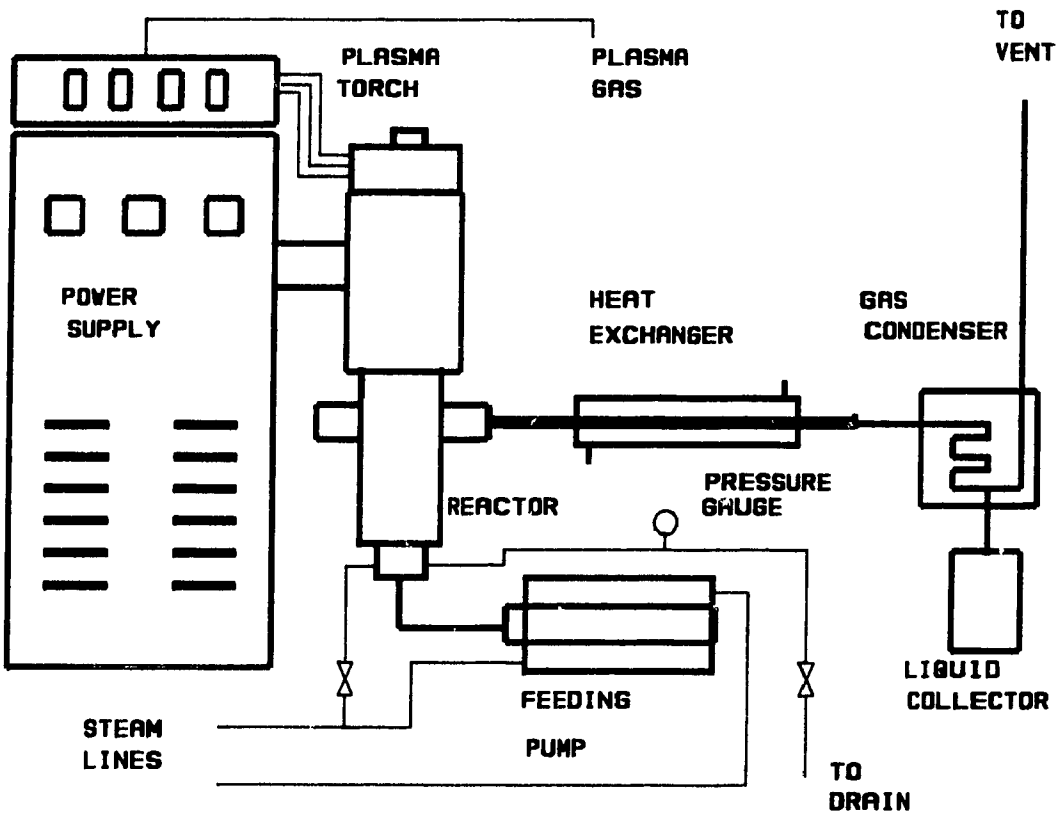

Figure 3.1

Schematic Diagram of the Experimental Apparatus.

of the torch; tangential injection of the gas was necessary to stabilize the plasma by confining it to the center of the tube and, thus, minimizing conductive heat loss to the tube and protecting the tube from the hot plasma. The ionized gas exited the torch through a water cooled copper nozzle 2.54 cm in diameter. The nozzle was equipped with two diametrically opposed holes 2 mm in internal diameter through which hydrogen was injected radially into the plasma tailflame.

3.1.2 Reactor and Feeding System

A laboratory-scale reactor was specially designed for the continuous pyrolysis of CANMET coprocessing residue. The reactor was designed to satisfy three important criteria: (1) plasma gases must have low residence time to avoid decomposition of gaseous products such as acetylene; (2) residue flow inside the reactor must have low Reynolds number to simulate the reaction of a micro droplet falling in a plasma flame; and (3) the reactor must have a well defined contact area between the residue and the plasma flame, and it must also provide flexibility in feeding and sampling.

The water-cooled inner part of the reactor was machined from stainless steel; it was 2.54 cm in diameter and 10 cm in length. It had two diametrically opposed gas outlets (1.27 cm in diameter) and a viewing port (1.91 cm in diameter) located 2 cm below the upper end of the reactor as shown in Figure 3.2. The gas exhausts were located in the top part of the reactor to shorten gas residence time and prevent

decomposition of acetylene and other hydrocarbons to carbon. The viewing port was perpendicular to the axis of the gas outlets, and it was kept clear by injecting argon gas (500 cm^3/min) to prevent deposition of carbon (soot) on the pyrex glass window. The reactor was joined to the lower end of the plasma torch with an O-ring seal tightened by six steel bolts.

The residue was fed to the reactor using a syringe pump consisting of a stainless steel syringe with steam-heated jacket, a variable d.c. motor and a gear box. The syringe total volume was 100 cm^3, and the pump could deliver flow rates ranging from 2 to 10 g/min. Steam at 860 kPa was used to heat the syringe and keep the residue in liquid form at about 450 K.

The residue was introduced into the reactor through an inconel tube 0.635 cm in internal diameter and 12 cm in length. The tube was made with a flat molybdenum tip (1.27 cm in diameter) to provide a larger and well-defined contact area between the plasma flame and the residue; this also prevented the flame from extending further down to the unreacted residue. The residue flowed into the reactor over the molybdenum tip in a fountain-like form creating a continuously renewed upper surface that was in complete contact with the plasma flame.

The lower part of the reactor (below the residue feed) provided a low temperature zone for the unreacted residue where it accumulated in a stainless steel collection

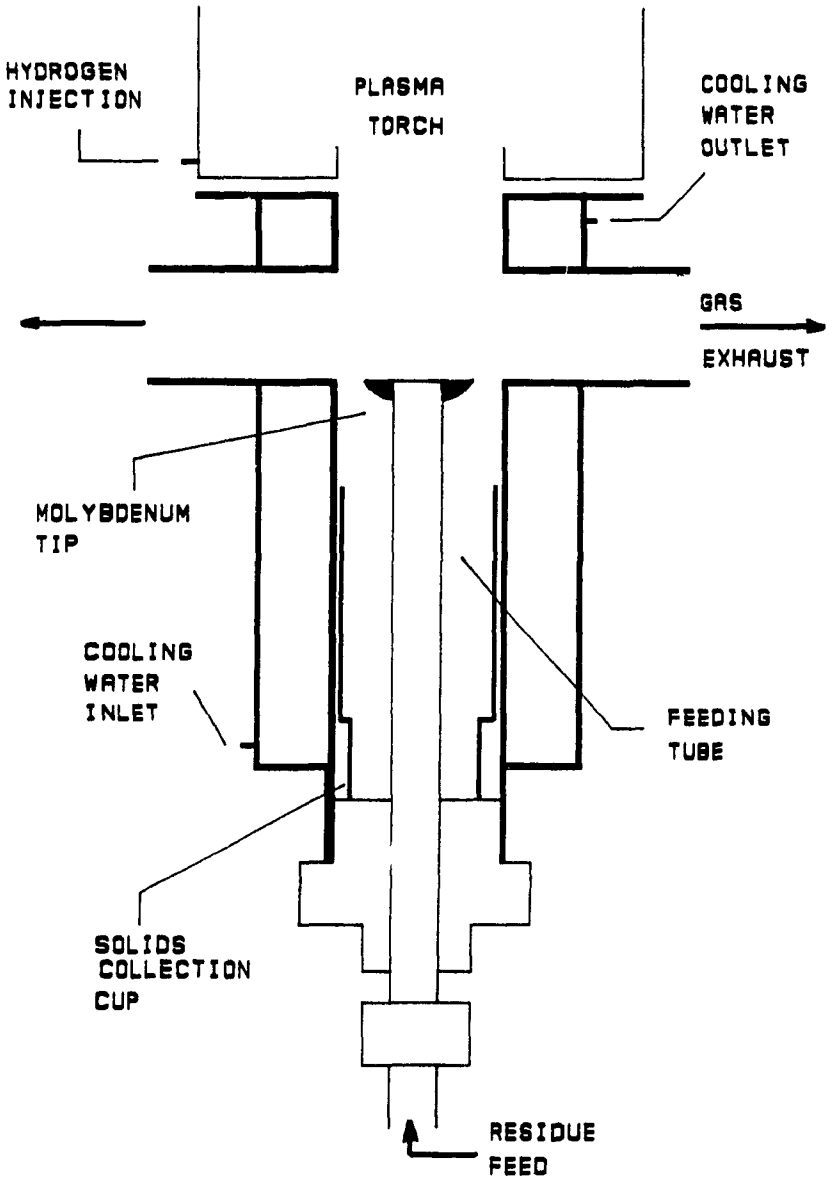

Figure 3.2

Cross-Sectional View of the Reactor.

cup. The bottom of the reactor also housed a support system for the feeding tube. The support system was designed to allow flexibility in positioning the tube, and it was steam heated to avoid solidification of the residue. The feeding tube was connected to the syringe pump through a short piece of teflon tubing 0.794 cm in internal diameter and 5 cm in length. The teflon tube was necessary to isolate electrically the reactor from the feeding system which was grounded. The teflon tubing was creating an elbow connection between the horizontal syringe and the vertical feeding tube, and it was continuously heated during experiments using an air heating gun to prevent solidification of the residue.

3.1.3 Sampling Probe

Gas samples were taken at different positions inside the reactor and at the gas outlets using a water-cooled suction probe previously used by Dlugogorski (1989). The probe was made of three concentric stainless steel tubes with diameters 1.6 mm, 3.2 mm and 6.4 mm, and it was 60 cm long. A Monostat varistaltic pump was used to withdraw gas samples at a constant flow rate.

3.2 EXPERIMENTAL PROCEDURE

After connecting the reactor to the plasma torch and fixing the feeding tube and the sampling probe to the desired positions, the following experimental procedure was

carried out:

1 - The power supply was turned on and allowed to warm up for about 20 minutes. At the same time, cooling water flow was started, and the system was checked for water leaks.

2 - A sample of the CANMET residue (about 120 g) was liquified by heating it in a 250 ml pyrex glass beaker in a microwave oven for about 15 minutes. The sample was then poured into the syringe which was connected to steam lines to keep the residue at constant temperature.

3 - The syringe was connected to the feeding tube by the teflon tubing, and argon gas flow was started to purge the reactor for about 1 minute (about 500 changes of reactor volume). The system was then checked for gas leaks.

4 - Plasma was initiated and the desired plate (input) power was set. Hydrogen gas was then injected into the plasma tailflame at the desired flow rate.

5 - The residue flow to the reactor was started. Once the residue was visible through the viewing window, a stop watch was started, and gas samples were taken every 30 seconds for about 3 minutes.

6 - The plasma torch, the residue flow and the stop watch were stopped at the same time. The power supply and the cooling water flow were turned off, and the gas samples were taken for analysis. The unreacted portion of the residue was weighed and collected in sampling vials for later analysis.

- 4 -

ANALYTICAL TECHNIQUES

4.1 PRODUCT GAS

Gas samples taken during experiments were analyzed with a Fisher gas partitioner Model 1200. A combination of two columns in series, Porapak N and a molecular sieve 5A (pore size 5 Å), was used for isothermal separation of the gaseous products at 353 K. This combination was used by Dlugogorski (1989) and was found to give satisfactory separation. The Porapak N was used to separate acetylene, ethane, ethylene and carbon dioxide. These gases by-passed the molecular sieve column which was used to separate hydrogen, nitrogen, methane, carbon monoxide and argon/oxygen. Oxygen and argon appeared at the same retention time and could not be separated. A longer column and a much lower temperature would be needed to separate these two gases. Oxygen and nitrogen in the product gas came only from air leaks during sampling. Estimates of the air leak (from nitrogen analysis) indicated that the amount of oxygen in the product gas was too small to affect the accuracy of argon analysis.

The partitioner was calibrated using a gas mixture containing argon (71.83 mol%), hydrogen (25.51%), nitrogen (0.40%), acetylene (1.48%), ethylene (0.49%), carbon monoxide (0.19%) and carbon dioxide (0.10%). There was no methane in the gas mixture; thus pure methane was used for methane-calibration. Calibration curves for these gases are given in Appendix A.

The carrier gas was a mixture of 91.5 % helium and 8.5% hydrogen, and its flow rate was fixed at 26 cm^3/min. The small fraction of hydrogen is needed to facilitate hydrogen detection (Kubanek, 1984). However, the presence of hydrogen in the carrier gas was found to cause difficulties in detecting small amounts of hydrogen. When samples of pure gases such as argon and nitrogen were analyzed, a small peak was observed at the same retention time as that of hydrogen. The peak area was found to increase linearly with increasing the volume injected as shown in Figure 4.1. This was believed to be due to disturbance of the carrier gas by the samples injected giving rise to the detection of hydrogen by the thermal conductivity detector (TCD). In order to correct for this disturbance, a fixed peak area of 3400, corresponding to the usual sample volume of 900 μl, was deducted from all hydrogen peak areas. Such correction was unnecessary for samples containing more than 15% hydrogen by volume.

4.2 ELEMENTAL ANALYSIS

The elemental composition of the CANMET residue and the unreacted solid particles was determined using the Control Equipment Corporation elemental analyzer Model 240-XA. The main components of the analyzer are a combustion tube, a reduction tube and a series of thermal conductivity detectors. The analyzer is accurate within ± 0.3% absolute.

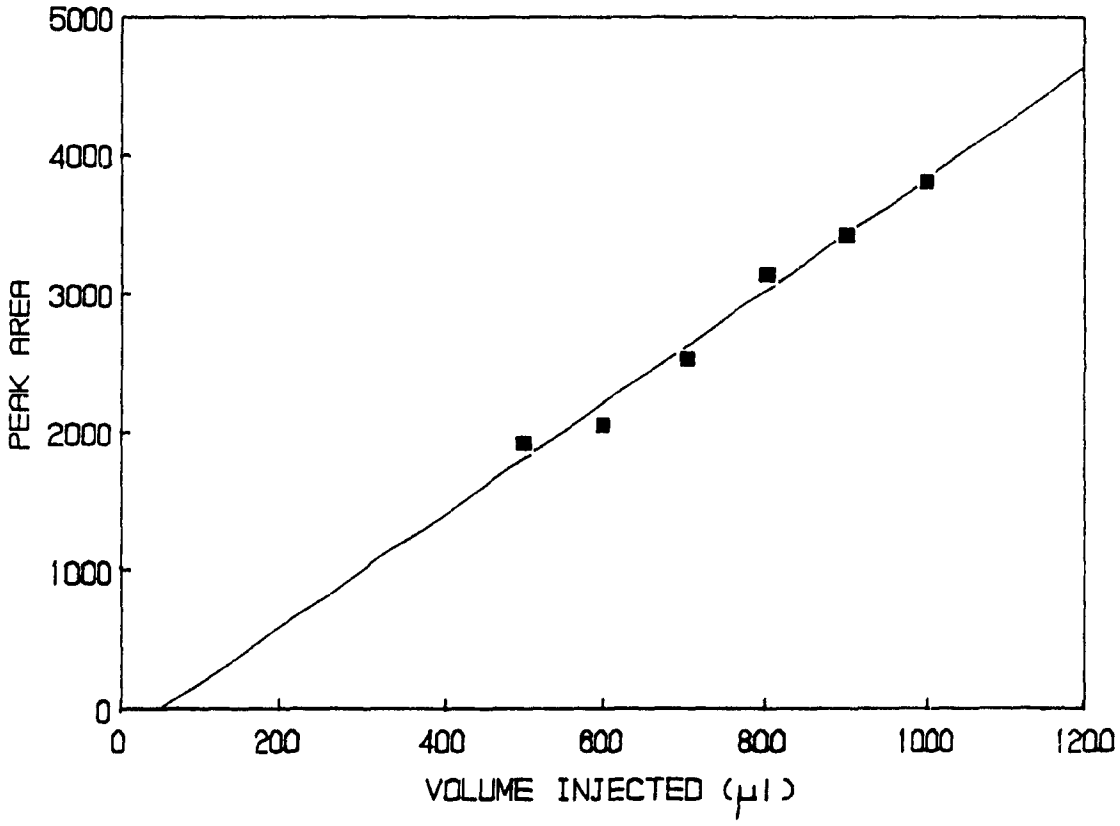

Figure 4.1

Variation of Peak Area of Apparent Hydrogen Volume of the Sample Injected.

For carbon-hydrogen-nitrogen analysis, a sample of 1-3 mg is accurately weighed (±0.0005 mg) and loaded into the analyzer. The sample is combusted in pure oxygen, and the products of combustion (water vapour, carbon dioxide, nitrogen oxides and other gases) are carried by helium through the reduction tube and then through the analytical train. In the reduction tube, nitrogen oxides are converted into molecular nitrogen. Water vapour is removed by a water trap located between the first pair of thermal conductivity cells. The change in signal by the detectors reflects the water or hydrogen content of the sample. Another trap between the following pair of detectors removes carbon dioxide and determines the carbon content. The nitrogen content of the sample is determined by the last two detectors.

For oxygen analysis, the combustion tube and the reduction tube were replaced with a pyrolysis tube containing platinized carbon and an oxidation tube containing copper oxide. The sample is pyrolysed in helium (at 1293 K) using platinized carbon to convert oxygen to carbon monoxide which in turn is converted to carbon dioxide by passing it through the copper oxide. Carbon dioxide is detected as described earlier. This gives the oxygen content of the sample.

For sulphur analysis, the combustion tube was replaced with a tube containing tungsten oxide packing, and the water trap was replaced with a tube containing silver oxide. The sample is combusted in oxygen (at 1123 K) using the tungsten oxide as a catalyst. Sulphur in the sample is oxidized to sulphur dioxide which is absorbed by

the silver oxide and then detected and measured in the same manner as hydrogen giving the sulphur content.

4.3 PLASMA TEMPERATURE

Direct measurement of plasma temperature through the use of thermocouples was not possible due to the high voltage r. f. field. Calorimetric measurements of the mean plasma temperature obtained by Dlugogorski (1989) were adopted for this work. Such measurements are valid as long as the torch efficiency is unaffected. To ensure that the efficiency is fixed, the plasma gas (argon) flow rate as well as the plate power grid setting were kept at the same values as those used by Dlugogorski. A plot of the mean plasma temperature versus input power is shown in Figure 4.2.

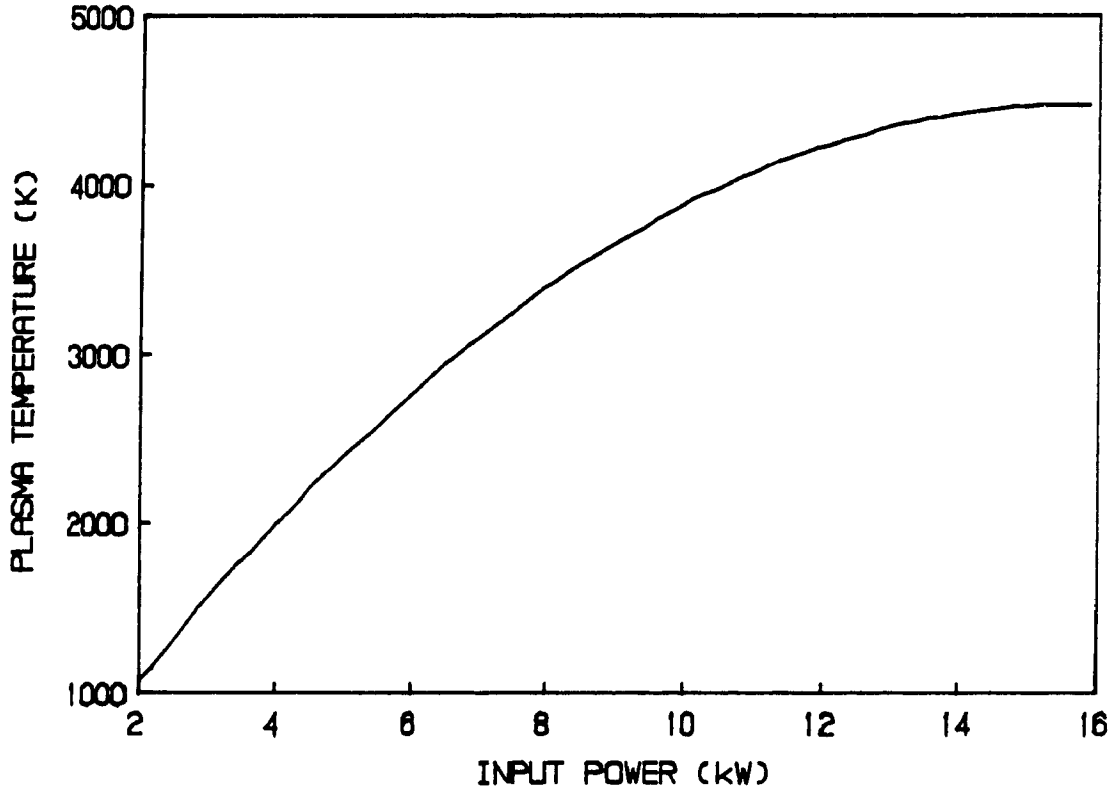

Figure 4.2

Variation of the Mean Plasma Temperature with Power Input.

(Based on data obtained by Dlugogorski, 1989)

- 5 -

ANALYSIS OF THE RESIDUE

The CANMET coprocessing residue is the residual pitch fraction collected as vacuum bottoms in the CANMET process. It contains most of the metals present in the heavy oil and the residual solids from the additives (catalyst). The residue is a black solid at room temperature and has a specific gravity of (1.25 ± 0.05). It starts to flow at a temperature of about 410 K.

The molecular structure of the residue is dictated mainly by that of the asphaltene fraction of the feed oil. Asphaltene is that fraction of heavy oil containing most of the metals, nitrogen and sulphur. It is this fraction that distinguishes heavy oil and makes it difficult to upgrade (Schumacher, 1982). An average asphaltene molecule consists of five or six units held together by their central aromatic discs and may have one or two nitrogen atoms and five or six sulphur atoms (Kubanek, 1985). The complex aromatic structure of asphaltene is inherited by the residue. Dlugogorski (1989) reported that the CANMET residue indeed contained a high proportion of condensed and complex aromatic hydrocarbons.

The elemental composition of the CANMET residue was determined using the Control Equipment Corporation analyzer Model 240-XA as described in Section 4.2. The ash content was determined by ashing samples of the residue at 1050 K to constant mass. Dlugogorski (1989) showed that ashing the residue at a higher temperature (1275 K) for few hours resulted in the transformation of all metal oxides to their highest and known levels of oxidations. A comparison of the elemental

analysis of the residue used in this work and that used by Dlugogorski is given in Table 5.1.

Table 5.1 Elemental Analysis of the CANMET Residue (wt %).

Element	Residue Used in This Work	Residue Used by Dlugogorski (1989)
Carbon	79.30	74.71
Hydrogen	6.33	6.60
Nitrogen	1.24	1.18
Sulphur	2.05	3.43
Oxygen	3.05	4.10
Ash	8.99	9.68
H/C	0.95	1.06

Although analyses for hydrogen and nitrogen are within analytical error (± 0.3% absolute), analyses for other elements and the ash content show that there is some difference between the two residues. When comparing the H/C ratios of both residues to those of a typical coal feed such as Forestburg coal (0.72) and a typical oil feed such as Cold Lake vacuum bottoms (1.38), one may conclude that higher coal concentration in the feed has resulted in the production of the residue used in this

work. Compared to that used by Dlugogorski, the residue used in this work was easier to feed, because it had lower viscosity at moderate and low temperatures; it was, however, more difficult to crack due to the lower hydrogen-to-carbon ratio. The lower levels of sulphur and ash in the residue studied here compared to those of the residue used by Dlugogorski could be attributed to a lower catalyst content of the coprocessing feed.

The effect of coal concentration in the CANMET coprocessing feed on the characteristics of the distillate products was studied by Rahimi et al. 1989. They found that increasing coal concentration resulted in higher molecular weight of the distillate and its hydrocarbon-type fractions. They also reported an increase in nitrogen content and a decrease in the sulphur content with increasing coal concentration. The effect of coal concentration on the characteristics of the residue has not been studied, and one can not use the Rahimi study to infer the change in the residue with varying coal content.

Although there is a difference in the elemental composition between the two residues, both residues have the same complex aromatic structure which, as was mentioned before, was inherited from the asphaltene fraction of the heavy oil. The difference in composition was mainly due to variations in the amount and content of the "additive" added in the coprocessing feed.

- 6 -

RESULTS AND DISCUSSION

The primary objective of this work was to study the continuous pyrolysis of CANMET coprocessing residue in r. f. plasma under different operating conditions. The study was an investigation of the effect of various parameters on the composition of the gaseous pyrolysis products and on the state of the residue after treatment. The parameters studied were plasma gas composition, plasma temperature and residue flow rate. Also, a laboratory-scale continuous reactor with a feeding system was specially designed and built for the study.

The composition of the gaseous products was the only dependent variable used for quantitative analysis because, as it will be shown in Section 6.5, in the system under investigation, the state of the residue after treatment was virtually unchanged. Thus, in this chapter most of the results will be based on the analysis of the product gas; analysis of the unreacted residue will be presented later in the chapter.

6.1 EFFECT OF PLASMA GAS COMPOSITION

Argon was the plasma gas used in all experiments, and its flow rate was fixed at 32,500 cm^3/min (at 298 K and 101.3 kPa); 64% of the gas was injected tangentially, while the rest was injected axially through a gas distributor on top of the plasma torch. Hydrogen was injected into the plasma tailflame ranging in molar percent of the total plasma gas from 0 to 23.

Dlugogorski (1989) found that at 33.5% hydrogen the deviation of the local hydrogen concentration from the mean concentration was about 13%. This deviation dropped to 5% at 27% hydrogen. In this work, the average deviation at 23% hydrogen was about 2% as determined by chromatographic analysis of gas samples taken from the reactor. This indicates that at 23% hydrogen, good mixing between hydrogen and the argon plasma was achieved.

6.1.1 Achievement of Steady State

The only gaseous products detected were acetylene, methane and ethylene. Although other gases (CO, HCN and H_2S) were predicted by thermodynamics (Section 6.6), none were found experimentally. The major product detected was acetylene; therefore its concentration in the exhaust stream was used to verify that steady state had been reached. Gas samples were taken at one of the reactor outlets using both the suction probe (1.6 mm internal diameter) and (for comparison) an uncooled 10 cm long copper tube with a much larger internal diameter (0.635 cm).

The system reached steady state after about one minute as shown in Figure 6.1. However, samples taken through the suction probe showed a decline in acetylene

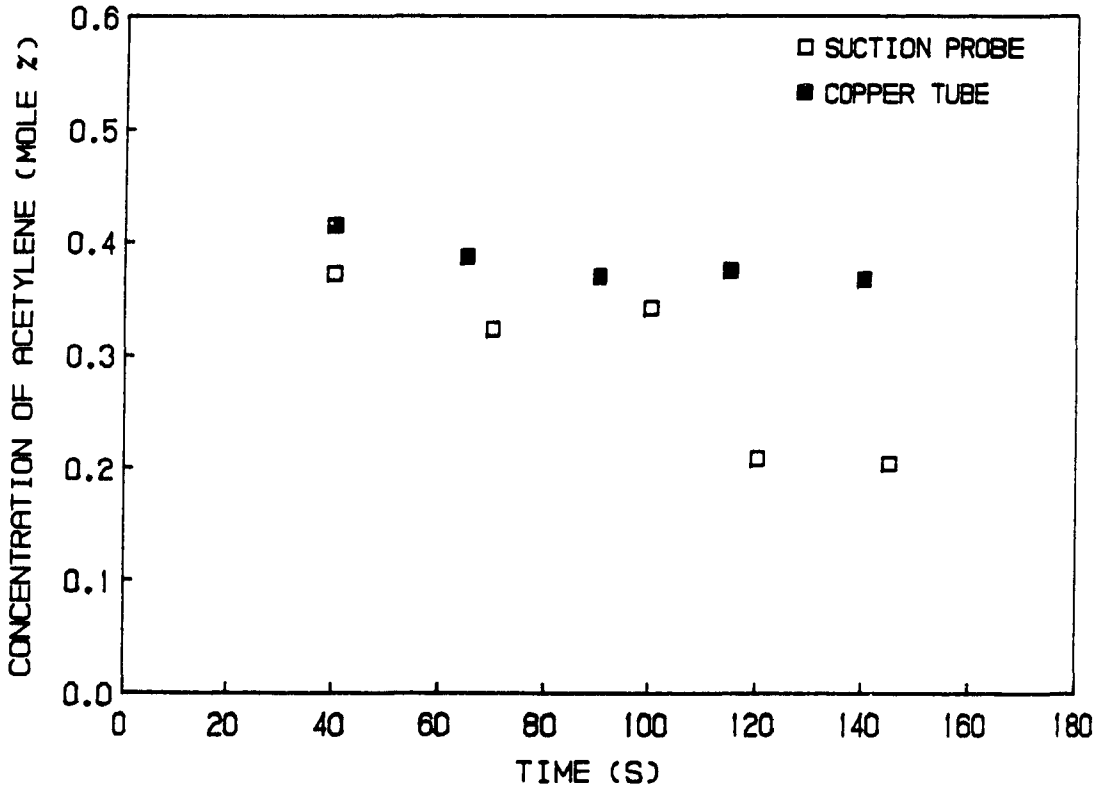

Figure 6.1

Variation of Acetylene Concentration in the product gas with Time. Power input = 9.02 kW; residue flow rate = 7 g/min; hydrogen molar concentration in the plasma gas = 20%

concentration after about two minutes. This was probably due to the fouling of the probe by soot sucked from the reactor. Soot deposition inside the probe lowers the flow rate and its cooling efficiency and reduces its quenching ability resulting in decomposition of acetylene. Thus, all experimental results were based on averaging samples taken (using the suction probe) within the first 100 seconds of run time.

6.1.2 Effect of Sampling Location

The suction probe was used to withdraw gas samples at different positions inside and outside the reactor along the central axis of the gas outlets at 2 cm intervals starting at one cm from the center of the reactor. The concentration of gaseous hydrocarbons in the exhaust stream was found to vary with sampling position as shown in Figure 6.2. This was attributed to two factors: residence time and mixing. Although short residence time is essential to avoid decomposition of products, a very short residence time may hinder the formation of such hydrocarbons as acetylene and ethylene (Gehrmann and Schmidt, 1971). The gas residence time at the first sampling point (less than 1 ms) was too short for most of the species in the gas phase to react. There was also less mixing (between reactive species released by the pyrolysis and hydrogen in the plasma) at the first point compared to the second sampling point; the first was located inside the reactor (just before the gas exits the reactor), while the second was located in an exhaust tube (1.27 cm in diameter) where the gas flow was turbulent (Reynolds number $\approx$ 2600) indicating good mixing.

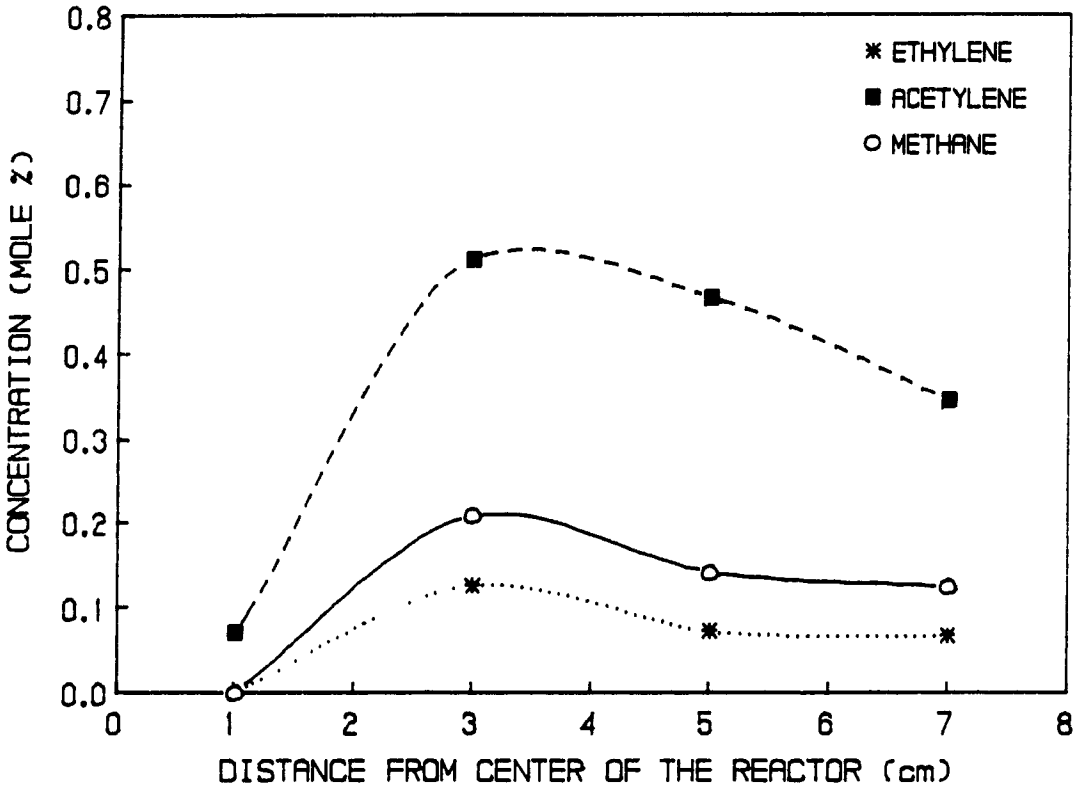

Figure 6.2

Variation of the Concentration of the Gaseous Hydrocarbons with Sampling Position. Power input = 9.02 kW; residue flow rate = 7 g/min; hydrogen molar concentration in the plasma gas = 20%

The other two sampling points were located along the same line at 5 and 7 cm from the center of the reactor. The decline in concentration beyond the second sampling point was mainly due to decomposition of gaseous hydrocarbons to carbon. The sampling positions (at 1, 3, 5 and 7 cm) shown in Figure 6.2 will be referred to through out the chapter as sampling points 1, 2, 3 and 4.

6.1.3 Effect of Hydrogen Addition on Heat Transfer

A calculation was carried out to see the effect of hydrogen addition on the rate of heat transfer from the plasma tailflame to the residue flowing over the tip of the feeding tube. In the calculation, radiative heat transfer was assumed to be constant, and since the objective was to see the profile of heat transfer as a function of plasma gas composition, only convective heat transfer was considered. The Nusselt number was estimated using the Whitaker equation for heat transfer to a sphere:

$$Nu = 2 + (0.4\ Re^{0.5} + 0.06\ Re^{0.67})Pr^{0.40}\ (\mu/\mu_s)^{0.25} \quad \text{..... (6.1)}$$

The residue flowing over the tip of the feeding tube was assumed to be a hemisphere with a diameter equal to the tip diameter. Since the residue surface was continuously renewed, its temperature was considered to be fixed at 473 K. All fluid properties except the gas surface viscosity were estimated at the mean plasma temperature. The plasma temperature was calculated as a function of plasma gas composition by

enthalpy balance of the argon plasma and the injected cold hydrogen; the calculated temperatures are plotted in Figure 6.3. It should be noted that the flat molybdenum tip of the feeding tube was always positioned within the core of the plasma jet (plasma tailflame); thus the temperature of the plasma gas surrounding the residue flowing over the tip was the true mean plasma temperature.

It is obvious that injection of hydrogen into the argon plasma tailflame lowers the plasma temperature and, consequently, lowers the argon enthalpy. At the same time, the thermal conductivity of the plasma increases because hydrogen has a much higher thermal conductivity than argon. However, at high concentration of hydrogen, the decrease in plasma temperature overcomes the increase in plasma thermal conductivity. Thus, one expects the convective heat transfer to reach a maximum at a moderate concentration of hydrogen. A plot of the calculated heat transfer versus plasma gas composition is shown in Figure 6.4. As expected, the profile shows a maximum between 10 and 15% hydrogen.

When the percent conversion of residue and the concentration of acetylene in the product gas were plotted against plasma gas composition, both curves were found to have profiles similar to that of the heat transfer rate as shown in Figures 6.5 and 6.6. The two curves in Figure 6.6 are for two sampling positions. The residue conversion shows a slightly higher scatter than the acetylene concentration because of the inaccuracy associated with weighing the unreacted portion of the residue.

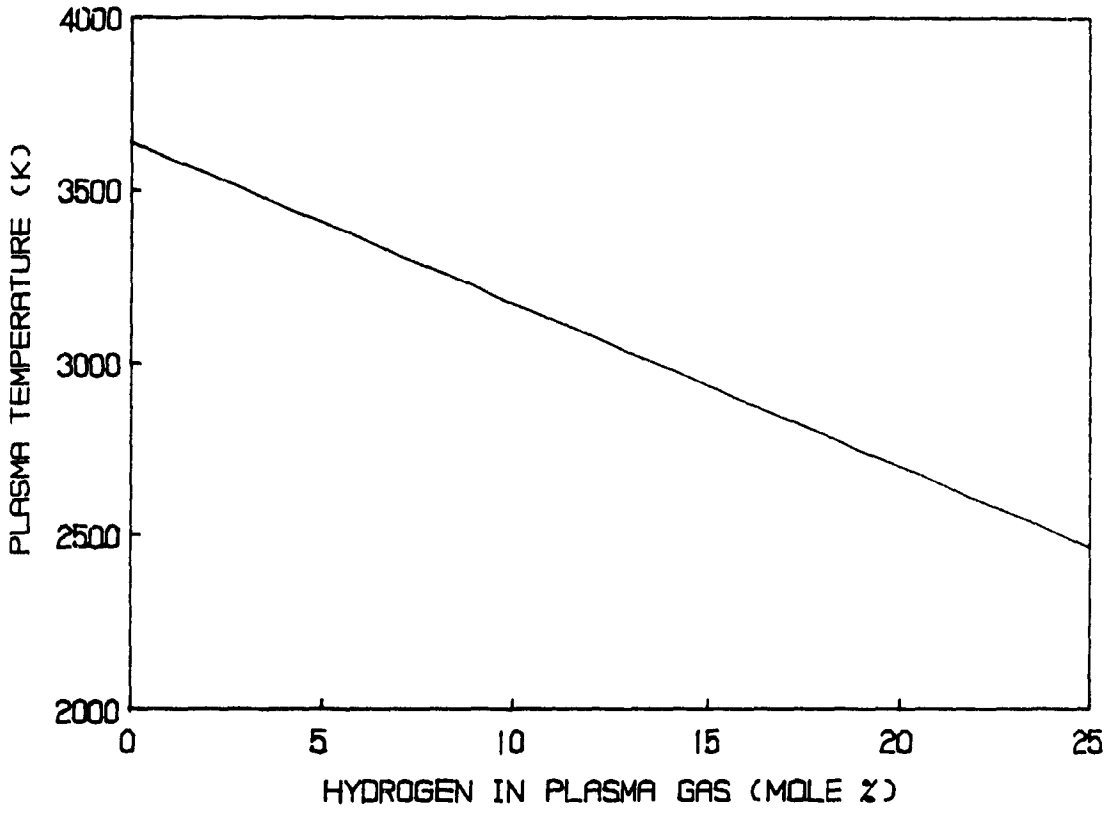

Figure 6.3

Calculated Plasma Temperature at Constant Power Input (9.02 kW) as a Function of Plasma Gas Composition.

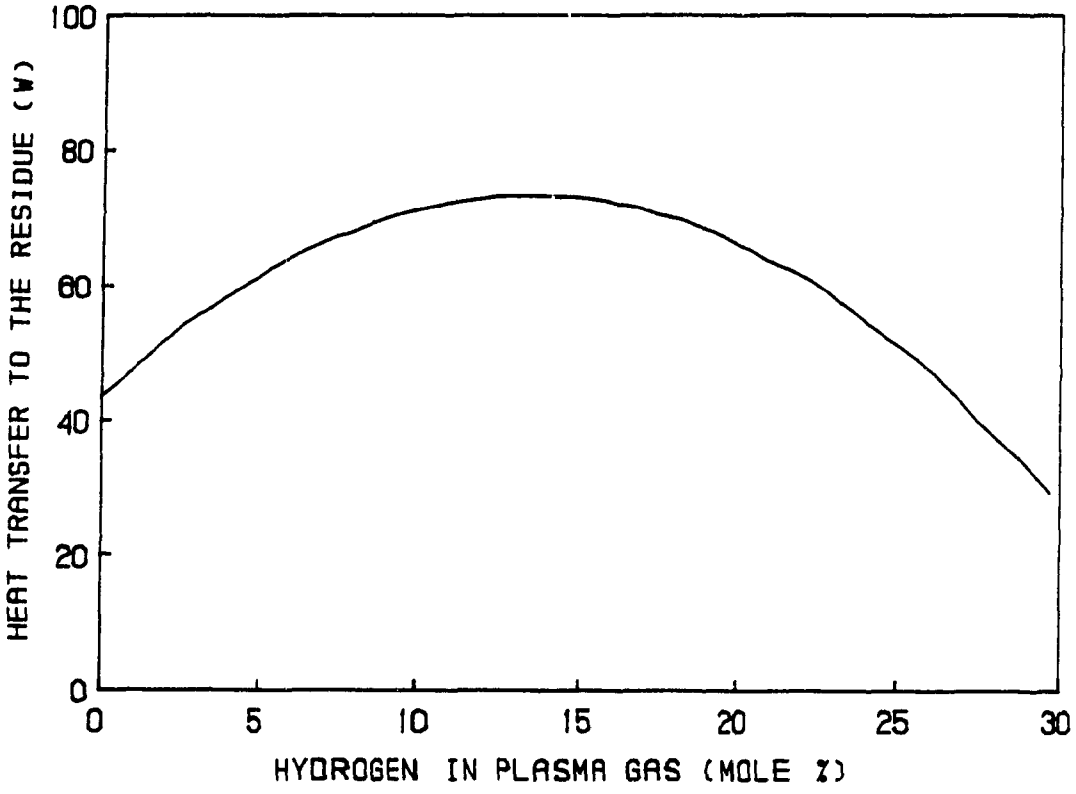

Figure 6.4

Calculated Heat Transfer at Constant Power Input (9.02 kW) as a Function of Plasma Gas Composition. The plasma temperature varies as shown in Figure 6.3.

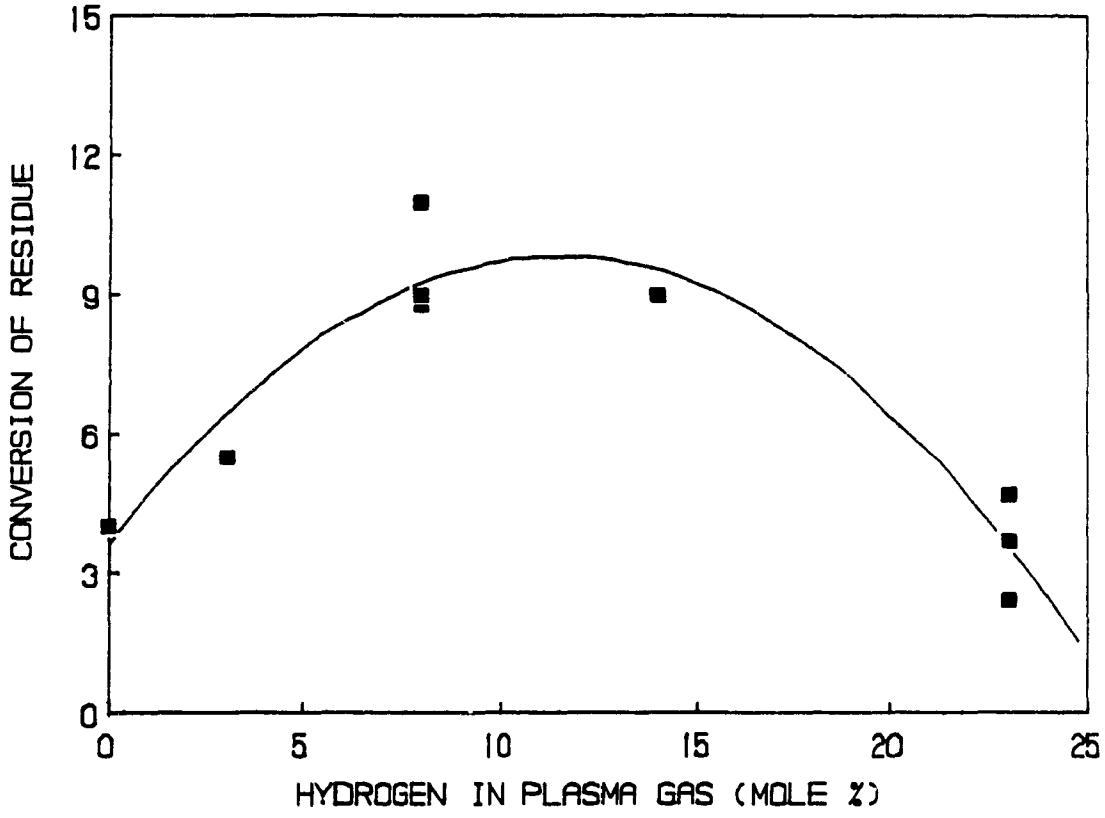

Figure 6.5

Effect of Plasma Gas Composition on Residue Conversion. Power input = 9.02 kW; residue flow rate = 7 g/min. The plasma temperature varies as shown in Figure 6.3.

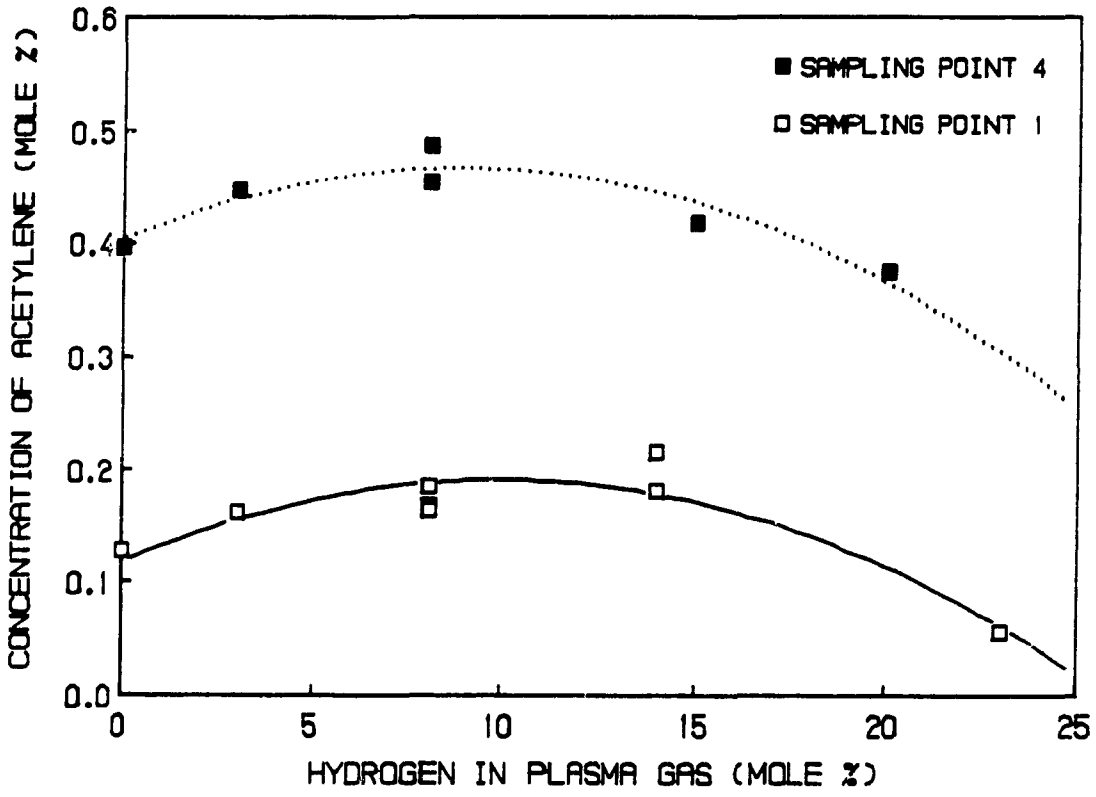

Figure 6.6

Effect of Plasma Gas Composition on Acetylene Concentration in the Product Gas. Power input = 9.02 kW; residue flow rate = 7 g/min. The plasma temperature varies as shown in Figure 6.3.

6.1.4 Yield of Gaseous Hydrocarbons

The agreement in profile among Figures 6.4, 6.5 and 6.6 suggests that the residue pyrolysis and the rate of acetylene formation are functions of heat transfer. One may consider that the formation of the gaseous products occurs through three different steps. The first is the pyrolysis of the residue; this is the boiling of the residue surface resulting in the thermal breakdown of the residue, the release of some radicals and the ejection of small residue droplets into the gas phase. The second is homogeneous gas phase reaction; this is the reaction of the released radicals with hydrogen. The third is heterogeneous reaction; this is the reaction of the ejected droplets or particles with hydrogen in the gas phase.

Although the ejected droplets (particles) may have a large surface area, their reaction is limited by the short gas residence time at low Reynolds number. Thus, their contribution to the gaseous products may be considered small relative to that of the homogeneous gas phase reaction. The rate of formation of gaseous products is believed to be controlled by the pyrolysis step which is strongly dependent on heat transfer.

The ratio of the amount of carbon converted to acetylene, methane and ethylene to the amount of carbon removed is plotted against plasma gas composition in Figure 6.7. This ratio will be referred to as the yield of hydrocarbons, and it can be written

as follows:

$$Y = \frac{C_h}{(C_h + C_d + E_p)} \qquad \text{..... (6.2)}$$

where,

C_h = moles of carbon converted to hydrocarbons (acetylene, methane and ethylene).

C_d = moles of carbon which deposited as carbon powder (carbon black).

E_p = moles of carbon ejected as small particles or droplets.

The moles of carbon converted to gaseous hydrocarbons (C_h) was determined through chromatographic analysis of the gaseous products. The moles of carbon deposited as carbon powder (C_d) and the moles ejected as small particles (E_p) could not be determined independently. They represent the balance of the moles of residue pyrolysed as determined by weighing the unreacted residue.

The amount of residue ejected into the gas phase as small particles or droplets (E_p) is a strong function of heat transfer. A higher rate of heat transfer results in faster and more vigorous boiling of the residue surface and, therefore, a higher rate of particle ejection. For a well quenched reaction and a short residence time at low and

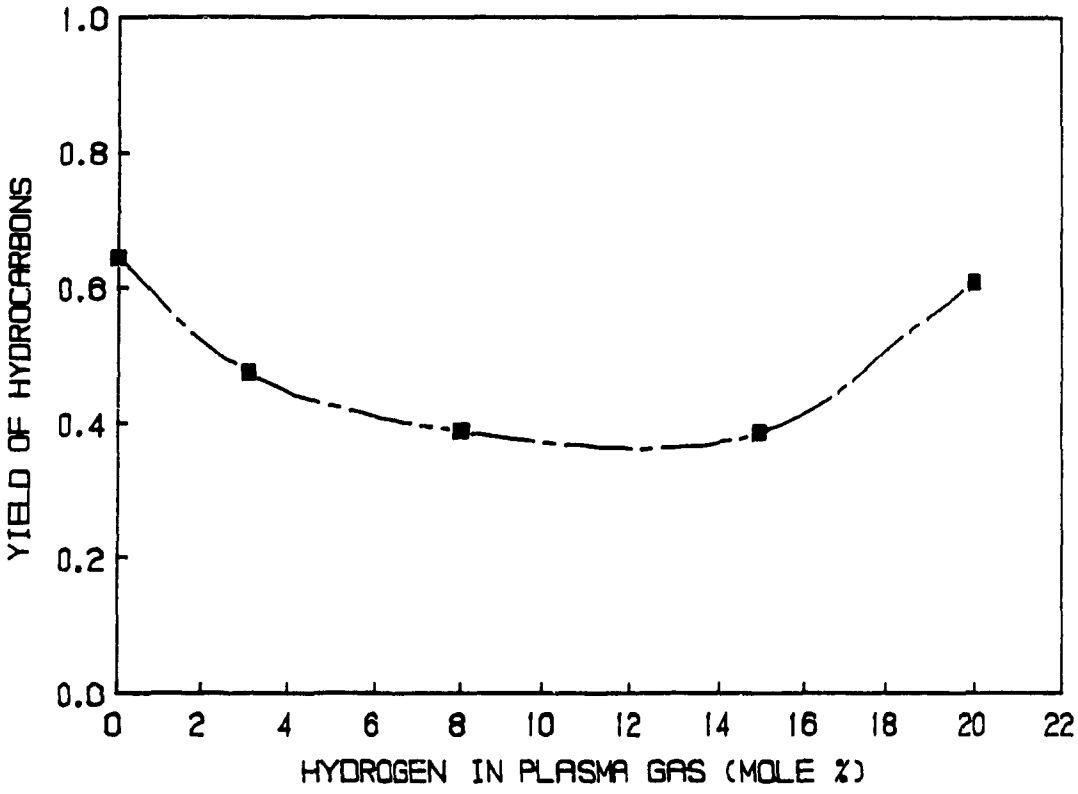

Figure 6.7

Effect of Plasma Gas Composition on the Yield of Hydrocarbons. Power input = 9.02 kW; residue flow rate = 7 g/min. The plasma temperature varies as shown in Figure 6.3.

moderate temperatures, the value of C_d is small relative to E_p and C_h. Thus, the yield (Y) reaches its highest value when E_p is small; that is when heat transfer is poor. On the other hand, Y reaches a minimum value when E_p is large relative to C_h; that is when the heat transfer rate is greatest. This was confirmed by experimental results as shown in Figure 6.7. Comparing this Figure with Figure 6.4, it is obvious that Y is at minimum when heat transfer is at maximum.

6.1.5 Deposition of Soot

Although carbon powder was observed at the reactor outlets, it was not possible to quantify its deposition rate or to relate it to the various operating conditions. The amount of carbon deposited in any single experiment was not sufficient for independent analysis. The powder, which will be referred to as soot, is a combination of deposited carbon (C_d) and partially reacted ejected particles (E_p). Samples of the soot were collected and analyzed. The analysis is given in Table 6.1. The presence of sulphur and nitrogen in the soot indicates that part of the soot comes from ejected particles.

The analyses given in Table 6.1 can be used to calculate the fraction of the soot which resulted from ejected particles. The sulphur and nitrogen analyses are not as accurate as those of carbon and hydrogen and can not be used with high confidence for such calculation. As a first approximation, one may assume that the particles do

not react in the gas phase and that they have the same composition as that of the original residue. Calculations based on the mass balance of carbon indicted that 35% of the soot came from ejected particles. However, the hydrogen balance calculations gave a value of only 26%. The disagreement between these calculations implied that some of the ejected particles had reacted while entrained in the gas phase. To determine the fraction that reacted (conversion) and the contribution of these particles to the soot formed, one could assume that hydrogen and carbon were removed from these particles, as they were entrained in the plasma gas, at an equimolar ratio to form acetylene.

When assuming that 28% of the ejected particles had reacted, both hydrogen and carbon balance calculations converged to a single value. The contribution of the ejected particles as determined by both calculations was 28% (detailed calculations are given in Appendix B). Thus, 72% of the soot resulted from deposited carbon (i.e. carbon black). It should be mentioned here that the calculations were based on a cumulative soot sample, and the results could vary with experimental conditions. Nonetheless, they give a good estimate of the range of the percentage of solids in the soot.

Table 6.1 Elemental Analysis of Soot and the CANMET Residue (wt%).

Element	Soot	CANMET Residue
Carbon	92.8	79.30
Hydrogen	1.63	6.33
Nitrogen	0.67	1.24
Sulphur	1.99	2.05

6.2 EFFECT OF PLASMA TEMPERATURE

The effect of plasma temperature on residue pyrolysis and on the composition of the gaseous products was investigated. The power input to the plasma torch was varied while plasma gas composition and residue flow rate were kept constant. Hydrogen was injected into the plasma tailflame so as its molar concentration in the plasma gas was 20%. Plasma temperature was related to input power through calorimetric measurements obtained by Dlugogorski (1989); a plot of temperature versus input power was previously shown in Figure 4.2. Calorimetry gives only the mean plasma temperature, and it is expected to be accurate within 200 K.

Gas samples were withdrawn at sampling point 2 (3 cm from center of reactor). At

this sampling position, gas temperature was lower than the mean plasma temperature. However, since the gas residence time was short (less than 2 ms), the effect of the slight decrease in temperature on the composition of the gaseous products was assumed to be negligible. Due to plasma torch limitations, it was not possible to operate with input power less than 9 kW or more than 14 kW. Below 9 kW, the plasma flame was inverted creating a relatively cold center surrounding the residue; this made it impossible to know plasma temperature or infer it from calorimetric data. Above 14 kW, the quartz tube confining the plasma inside the torch broke due to the high coupling energy.

Although the amount of carbon removed from the residue increased with increasing temperature as shown in Figure 6.8, the fraction converted to hydrocarbon gases (Y) decreased beyond 3000 K as shown in Figure 6.9. This can be due to a combination of two different factors. Hydrocarbon gases, especially acetylene, are less stable at high temperature; they decompose to carbon which precipitates as carbon powder (C_d). This was observed experimentally (Figure 6.10); it was also determined by thermodynamic calculations (Figure 6.14). Also, the amount of carbon ejected into the gas phase as small droplets (particles) increases with increasing temperature. Thus, the denominator in Equation 6.2 rises as temperature is increased above 3000 K resulting in the decline of the yield. The low range of temperatures (below 2700 K) could not be tested due to the torch limitations mentioned earlier.

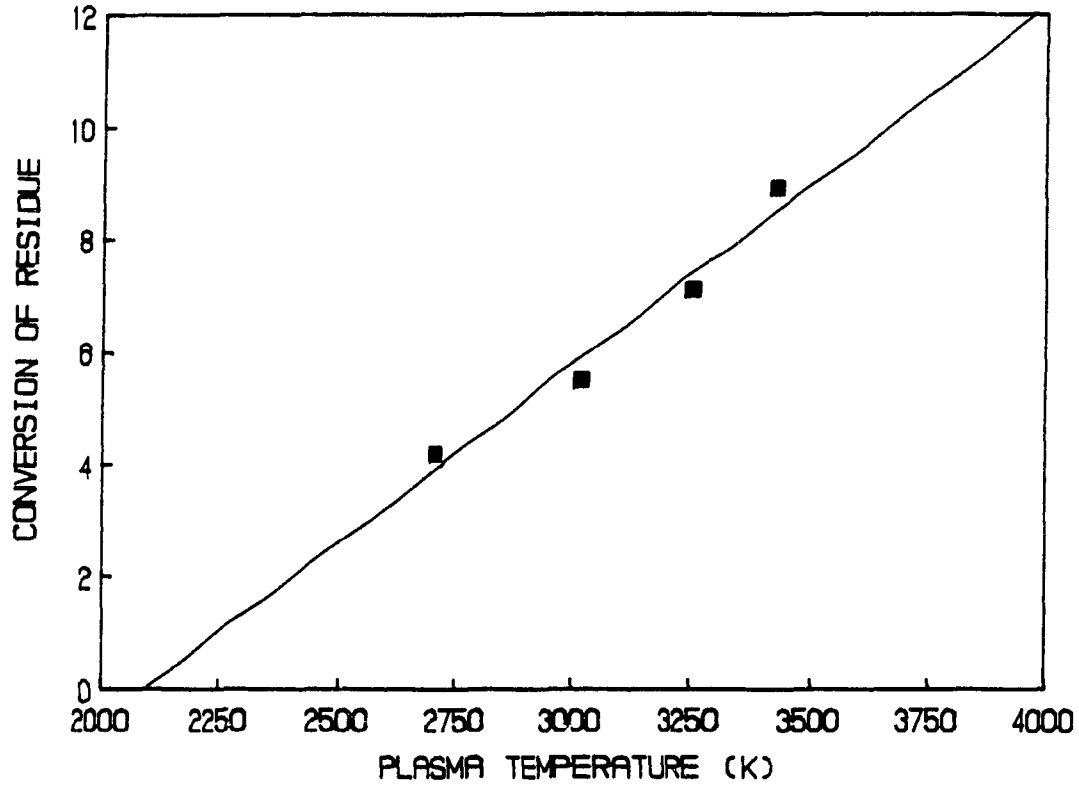

Figure 6.8

Effect of Plasma Temperature on Residue Conversion. Residue flow rate = 8 g/min; hydrogen molar concentration in the plasma gas = 20%.

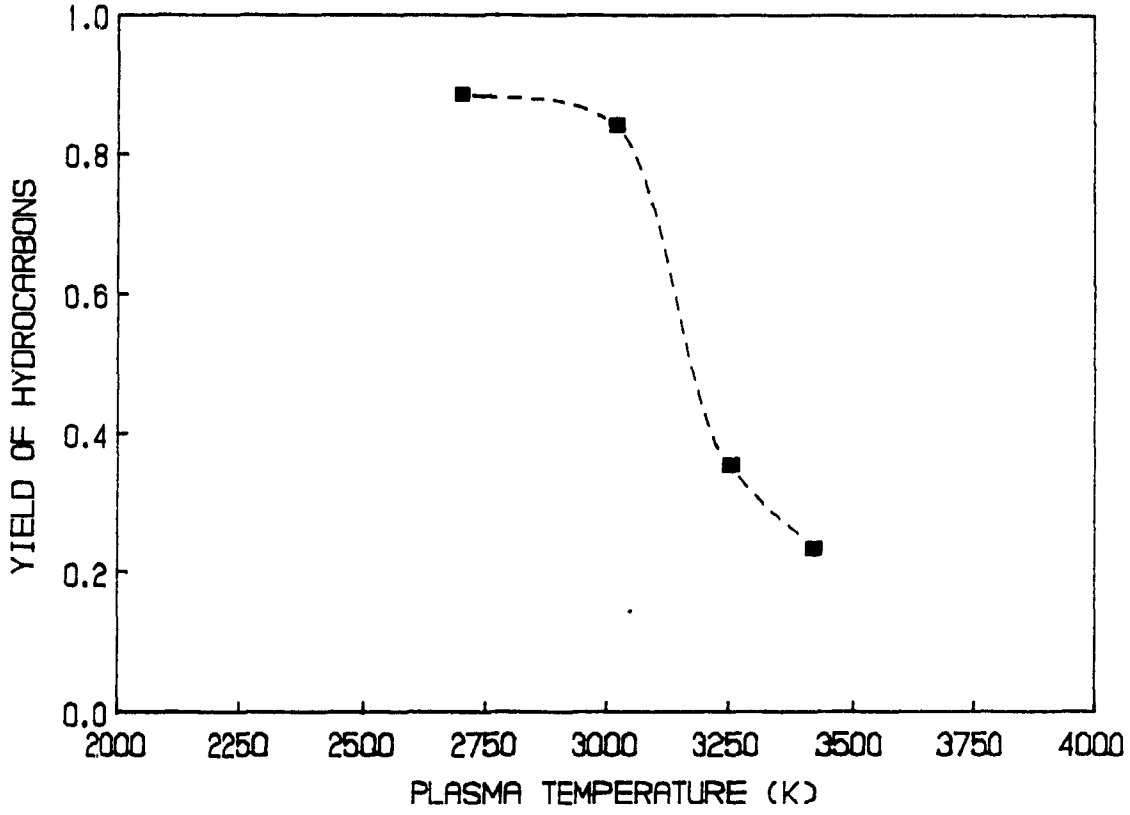

Figure 6.9

Effect of Plasma Temperature on the Yield of Hydrocarbons. Residue flow rate = 8 g/min; hydrogen molar concentration in the plasma gas = 20%.

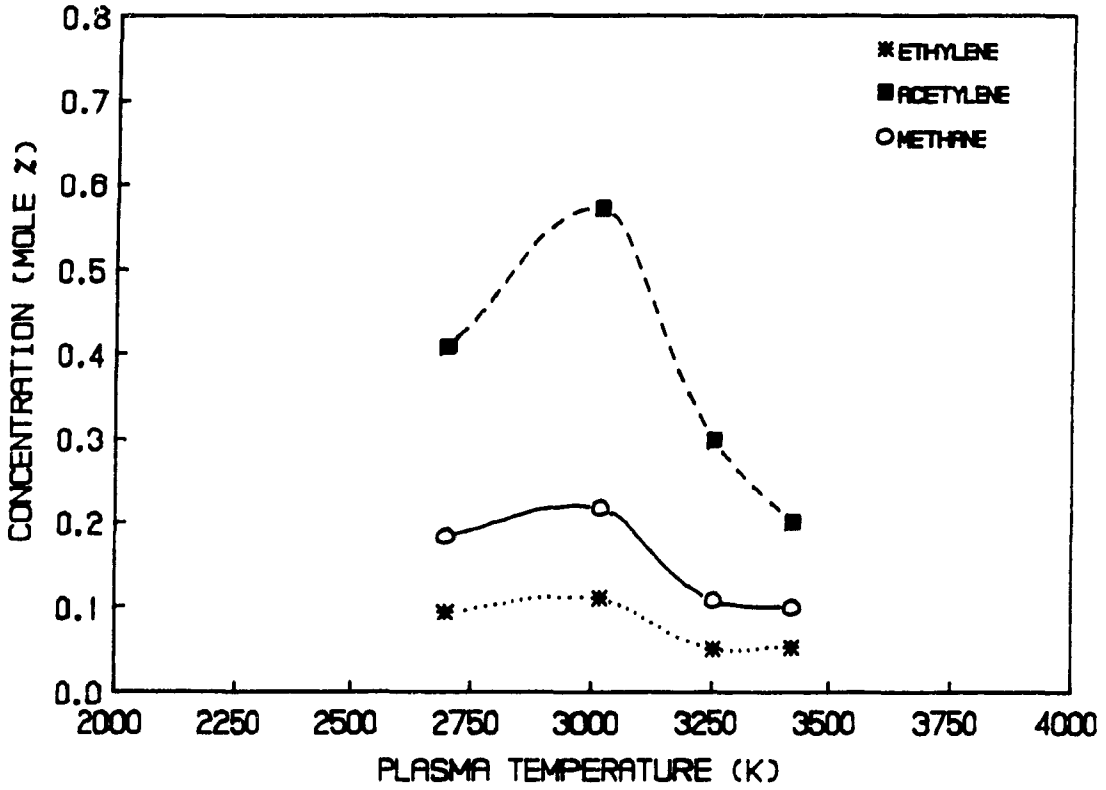

Figure 6.10

Effect of Plasma Temperature on the Concentration of Gaseous Hydrocarbons in the product gas. Residue flow rate = 8 g/min; hydrogen molar concentration in the plasma gas = 20%.

6.3 EFFECT OF RESIDUE FLOW RATE

A syringe pump was used for feeding the residue at flow rates ranging from 2 to 10 g/min. It was not possible, however, to operate through the whole range. At low flow rates (less than 6 g/min), the residue pyrolysed rapidly creating a dome of solids on top of the feeding tube and preventing further flow. A similar problem was encountered at moderate flow rates with high plasma temperatures; in this case, the liquid residue trickled below the dome of solids virtually unreacted. Operation at high flow rates (greater than 9 g/min) was not possible, because the solids collection cup in the lower part of the reactor (Figure 3.2) filled up with the unreacted residue before the system could reach steady state.

A few experiments were conducted ranging in flow rate from 6 to 9 g/min. The hydrogen molar concentration in the plasma gas was fixed at 8% giving a plasma temperature of 3246 K. Both the amount of residue converted and the concentration of acetylene in the product gas decreased with increasing flow rate as is shown in Figures 6.11 and 6.12. This was expected, because high flow rate resulted in less contact time between the residue and the plasma and, consequently, less residue reacted. However, since the plasma temperature and plasma gas composition were fixed, the rate of heat transfer was virtually unchanged, and hence the overall change in acetylene concentration was negligible.

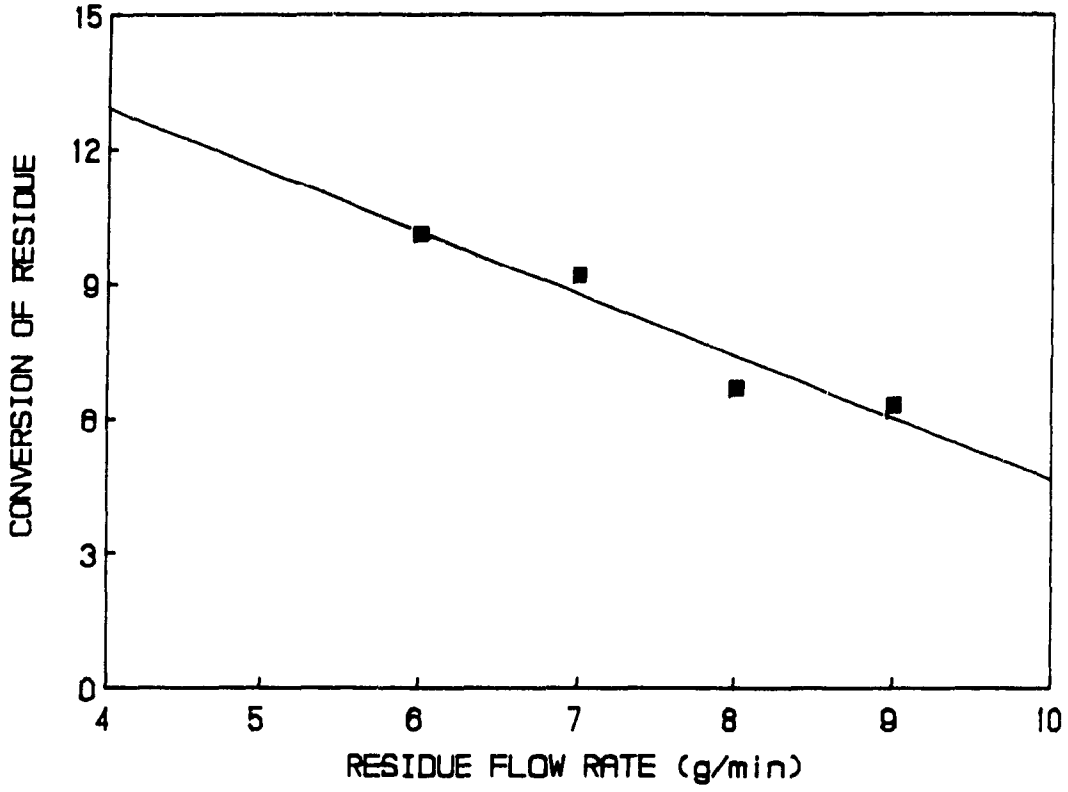

Figure 6.11

Effect of Residue Flow Rate on Residue Conversion. Power input = 9.02 kW; hydrogen molar concentration in the plasma gas = 8%.

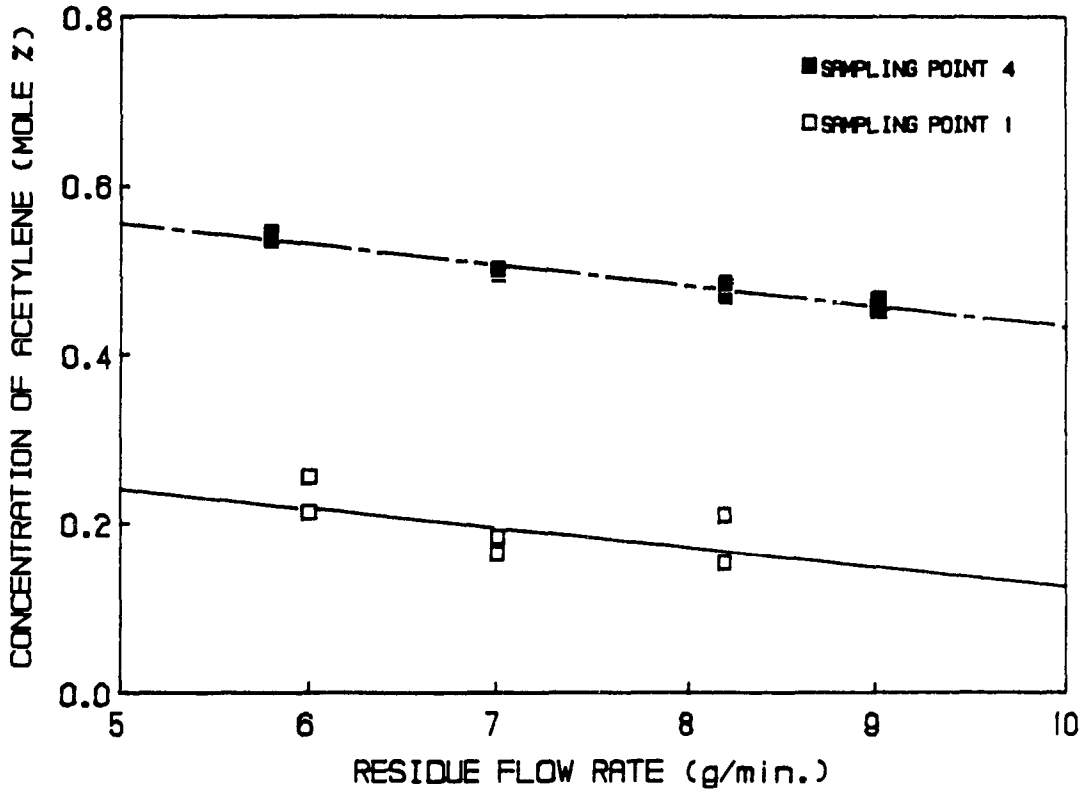

Figure 6.12

Effect of Residue Flow Rate on Acetylene Concentration in the Product Gas. Power input = 9.02 kW; hydrogen molar concentration in the plasma gas = 8%.

6.4 ISOLATION OF LIQUID HYDROCARBONS

Although the exhaust gases were passed through a tube immersed in a slurry of dry ice in acetone at 216 K to condense any liquid hydrocarbons, no liquids were isolated. The conversion of high molecular weight hydrocarbons to liquids was studied by Baronnet et al (1987). They found that the conversion depended mainly on molecular structure. High molecular weight cycloalkanes and aromatics had higher conversion (12%) than did long chain paraffins (2%). The CANMET residue is mainly composed of complex aromatics rather than aliphatics and cycloalkanes. Thus, the residue composition is believed to be the prime reason for the absence of liquid products.

A recent study of low temperature hydropyrolysis of heavy oils showed that conversion to liquid hydrocarbons was mainly dependent on reaction temperature (Hikita et al, 1989). Increasing reaction temperature (greater than 1073 K) increased the conversion to gaseous products and decreased that to liquids. Although the study was carried out for long residence times and at low temperatures, it could indicate that the plasma temperatures in this work (greater than 2700 K) were too high for the production of liquid hydrocarbons from hydropyrolysis of CANMET residue.

6.5 ANALYSIS OF UNREACTED RESIDUE

Samples of the unreacted residue, collected at the bottom of the reactor, were analyzed to determine the effect of the various operating condition on the state of the residue after treatment. The carbon, hydrogen and nitrogen content of the unreacted residue did not show any change with the varying operating conditions. It remained about the same (within analytical error) as that of the original, untreated CANMET residue. A plot of the C-H-N content of the unreacted residue versus plasma gas composition is shown in Figure 6.13. This indicated that the pyrolysis was uniform, and that there was no preferential removal of carbon, hydrogen or nitrogen. The unreacted residue was ashed at 1050 K to constant mass, but no appreciable change in the ash content was found. This was probably due to the low overall residue conversion (less than 10%). One would expect the ash content of the residue to increase at high conversion. Although the pyrolysis may still be uniform at high conversion (no preferential removal of one element of carbon, hydrogen or nitrogen over the other two), the C-H-N content of the unreacted residue is expected to be lower than that of the original, untreated CANMET residue.

6.6 THERMODYNAMIC ANALYSIS

The thermodynamic analysis of plasma pyrolysis of the CANMET residue was carried out by Dlugogorski (1989). In this section, the equilibrium composition of the

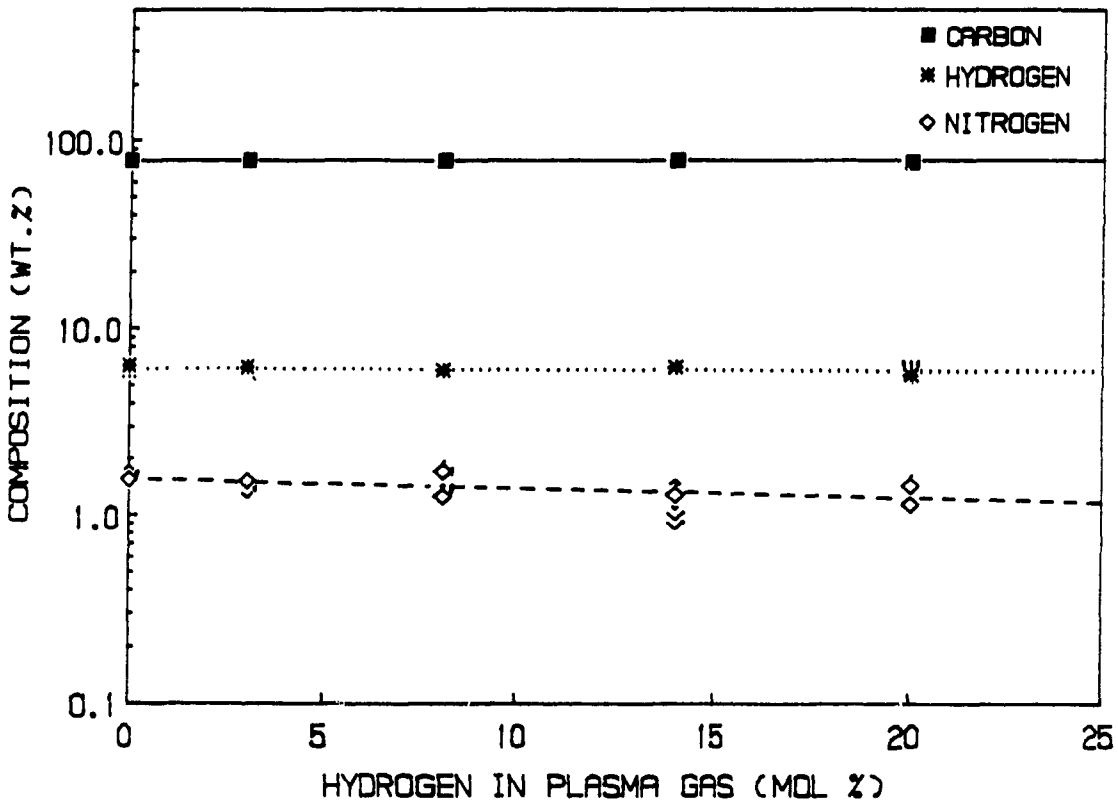

Figure 6.13

Variation of the C-H-N Content of the Unreacted Residue with Plasma Gas Composition. Power input = 9.02 kW; residue flow rate = 7 g/min. The temperature varies as shown in Figure 6.3.

continuous plasma pyrolysis is investigated. In thermodynamic analysis, it is assumed that the residue is exposed to plasma conditions for an unlimited period of time until the system reaches equilibrium. This assumption may hold for single particle batch pyrolysis, but it is not valid for continuous pyrolysis. In continuous plasma pyrolysis, the residue is exposed to the plasma for only a short period, and only part of the residue gets to react. Thus, the objectives of the calculations were to predict the thermodynamic equilibrium composition as a function of plasma temperature and plasma gas composition for the specific conditions studied in this work and to compare such predictions with experimental results. The elemental composition of the organic part of the residue given in Table 5.1 was used for the calculations.

Calculations were carried out using **F.A.C.T.** computer program which had several sub-programs. Only two of these programs were used: DATAENTRY and EQUILIB. The latter calculates equilibrium composition using the minimization of Gibbs free energy developed by White et al (1958). For a fixed temperature and pressure, the Gibbs free energy is minimized in terms of the number of moles. The program requires the standard heat of formation (at 298 K), the absolute entropy (at 298 K) and the heat capacities as a function of temperature as input. Details about the calculation of equilibrium composition using the minimization of Gibbs free energy or other methods can be found in the text of Smith and Missen (1982).

DATAENTRY is used for creating data files. For this calculation, a data file created by Dlugogorski (1989) was used. Using data from JANAF tables (1971), Dlugogorski fitted the heat capacities for some carbon, hydrogen, nitrogen, sulphur and oxygen containing compounds into the following form:

$$Cp(T) = A + B*10^{-3} T + C*10^{5} T^{-2} + D*10^{-6} T^{2} \quad (6.3)$$

Values of A, B, C and D for the various compounds are given in Appendix C in Table C.1 for the temperature range (298 - 2000 K) and in Table C.2 for the temperature range (2000 - 6000 K).

6.6.1 Plasma Temperature

The equilibrium composition was calculated for plasma temperature ranging from 2200 to 4000 K for a fixed hydrogen molar concentration in the plasma gas of 20%. The calculations were based on the amount of residue determined experimentally to have reacted as a function of plasma temperature (Figure 6.8); therefore the reaction stoichiometry varied with plasma temperature. The specific conditions (moles of residue reacted and molar ratio of argon to hydrogen to residue) at the temperatures used in the calculations are listed in Table 6.2. All calculations discussed in this section were based on the assumption that only gaseous products were present at equilibrium. The effect

of including graphite as a solid phase on the equilibrium composition will be discussed later.

Table 6.2 Conditions for Thermodynamic Calculations of Equilibrium Composition as a Function of Plasma Temperature.

Plasma Temperature (K)	Moles of Residue Reacted	Molar Ratio Ar : H_2: Residue
2200	0.0042	1 : 0.25 : 0.0028
2500	0.0151	1 : 0.25 : 0.0102
3000	0.0333	1 : 0.25 : 0.0224
3500	0.0515	1 : 0.25 : 0.0346
4000	0.0697	1 : 0.25 : 0.0469

A plot of the calculated equilibrium composition as a function of plasma temperature is shown in Figure 6.14. In agreement with experimental results (Figure 6.10), the concentration of acetylene as the major gaseous hydrocarbon product reaches maximum between 2800 and 3200 K. Other hydrocarbons (CH_4 and C_2H_4) decline sharply with increasing plasma temperature. This is due to the instability of these gases at high temperature; they decompose at high temperature to form soot.

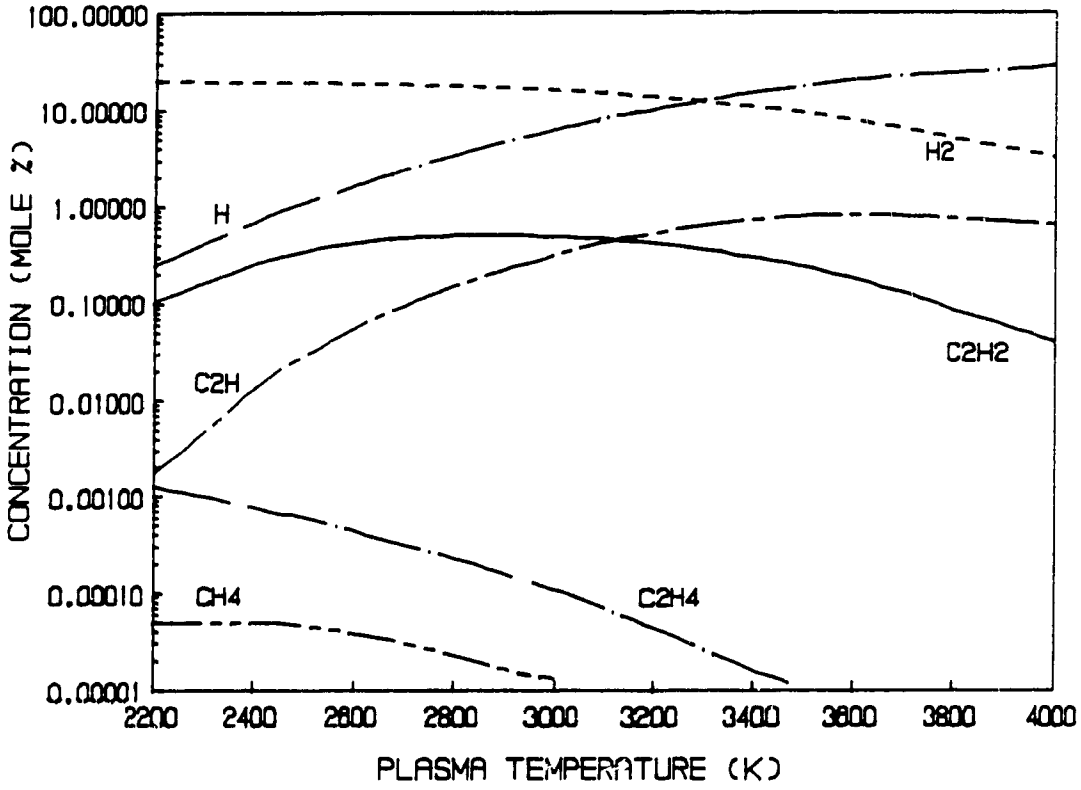

Figure 6.14

Variation of the Predicted Equilibrium Composition with Plasma Temperature. Hydrogen molar concentration in the plasma gas = 20%. The reaction stoichiometry varies as shown in Table 6.2.

6.6.2 Plasma Gas Composition

The calculated equilibrium composition is plotted against plasma gas composition in Figure 6.15. The calculations were based on the amount of residue determined experimentally to have reacted as a function of plasma gas composition Figure 6.5. Again, all calculations were based on the assumption that only gaseous products were present at equilibrium.

As was mentioned in Section 6.1.3, the plasma enthalpy was lowered by the addition of cold hydrogen; consequently, the plasma temperature could not be fixed while varying plasma gas composition. The temperature declined with increasing hydrogen in the plasma gas as shown in Figure 6.3. Thus, as a result of varying plasma gas composition, both the reaction stoichiometry and plasma temperature were varied simultaneously. The conditions, at which equilibrium composition was calculated as a function of plasma gas composition, are listed in Table 6.3.

The concentration of acetylene at equilibrium increased with hydrogen addition reaching a maximum at 13% hydrogen and then stabilized. Although this showed some agreement with experimental results, the concentration of acetylene was found experimentally to decline after reaching a maximum at about 13% hydrogen as shown in Figure 6.6. This slight disagreement at high hydrogen concentration was due to the fact that thermodynamic calculations were based on the assumption that all

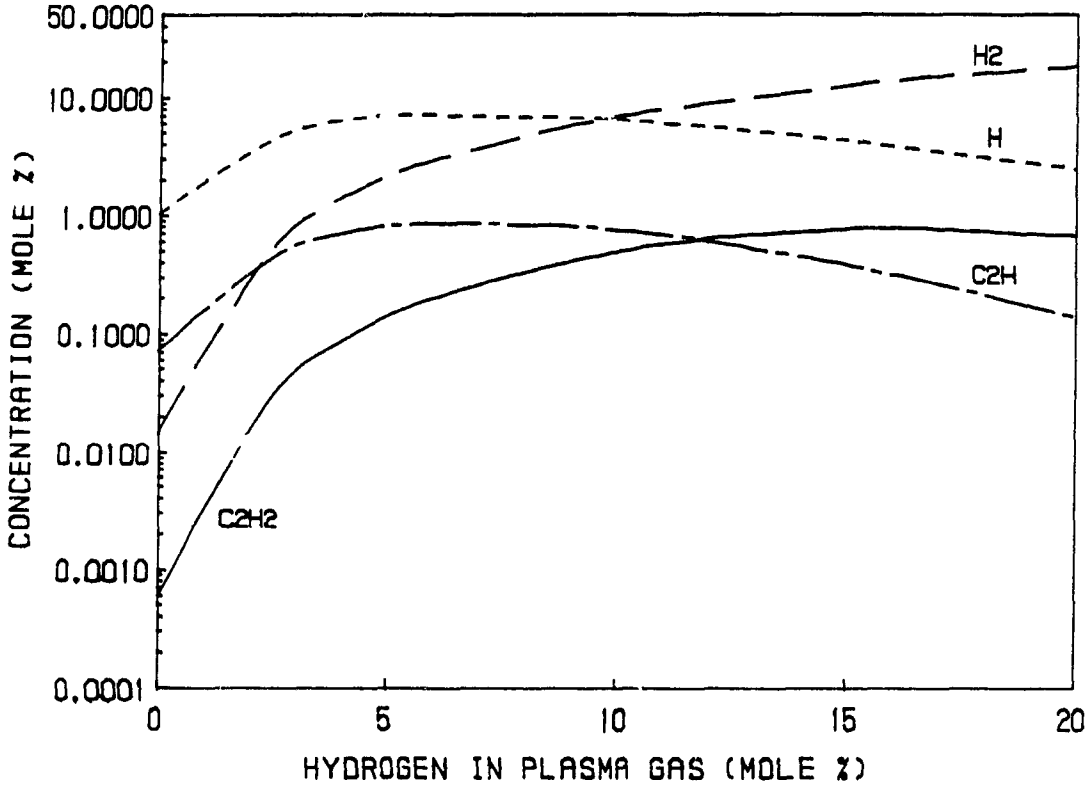

Figure 6.15

Variation of the Predicted Equilibrium Composition with Plasma Gas Composition. The temperature and the reaction stoichiometry vary as shown in Table 6.3.

residue was converted to gaseous products (no solid carbon was present), while experimentally some of the residue was ejected in the form small droplets which remained virtually unreacted or deposited as soot. At high hydrogen concentrations, plasma temperature decreases to levels where acetylene is less stable and solid carbon becomes predominant. The difference between the calculated equilibrium compositions with and without solid carbon (graphite) is shown in Figure 6.18.

Table 6.3 Conditions for Thermodynamic Calculations of the Equilibrium Composition as a Function of Plasma Gas Composition.

H_2 in Plasma Gas (mol %)	Plasma Temp. (K)	Moles of Res. Reacted	Molar Ratio AR : H_2: Res.
0	3669	0.0183	1 : 0.00 : 0.0123
3	3504	0.0324	1 : 0.03 : 0.0218
8	3246	0.0465	1 : 0.09 : 0.0313
15	2916	0.0464	1 : 0.18 : 0.0313
20	2700	0.0322	1 : 0.25 : 0.0217

The concentration of other hydrocarbon gaseous products (CH_4 and C_2H_4) was so small compared to that of acetylene that they were not included in Figure 6.15. Other species abundant at equilibrium were H and C_2H; the presence of H even at

0% hydrogen implies that this radical is released by the pyrolysis of the residue. Both H and C_2H followed parallel profiles which indicates that they are simultaneously released through the decomposition of hydrocarbons in the residue. It is believed that with rapid quenching C_2H combines with H or H_2 in the gas phase to form acetylene (Plooster and Reed, 1959).

6.6.3 Production of CO, HCN and H_2S

Some highly toxic gases were predicted by thermodynamic calculations. These include CO, HCN and H_2S. The equilibrium composition of CO and HCN as a function of plasma temperature and plasma gas composition is shown in Figures 6.16 and 6.17 respectively. Although some H_2S was present at equilibrium, its concentration was so small (less than 2 ppm) relative to those of the other two gases that it was excluded from the figures.

Both CO and HCN showed similar responses to changes in plasma gas composition. Both increased with hydrogen addition reaching a maximum at moderate hydrogen concentration (10 - 15%) and then declined. One can only attribute this to the changes in heat transfer by hydrogen addition. As was mentioned earlier, the reaction stoichiometry in the thermodynamic calculations were based on the number of moles determined to have reacted through experiments (Tables 6.2 and 6.3). It was also found (section 6.1) that the amount of residue removed by pyrolysis (residue

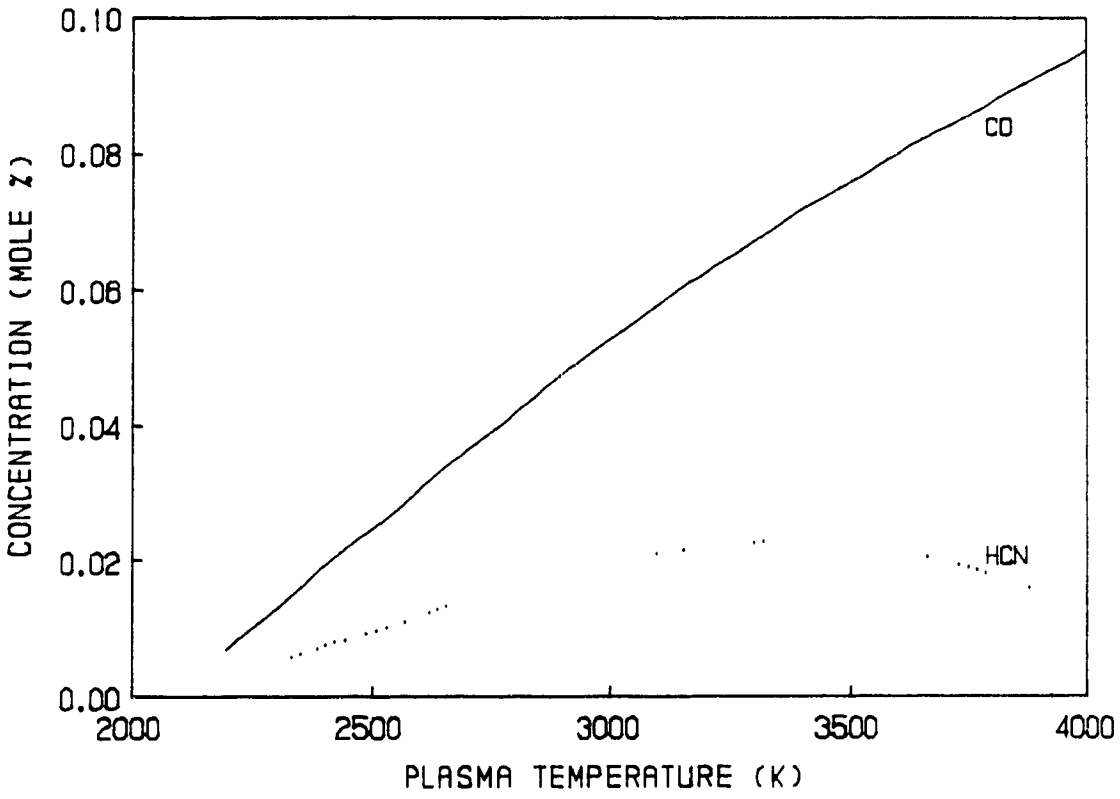

Figure 6.16

Variation of the Predicted Equilibrium Concentration of CO and HCN with Plasma Temperature. The reaction stoichiometry varies as shown in Table 6.2.

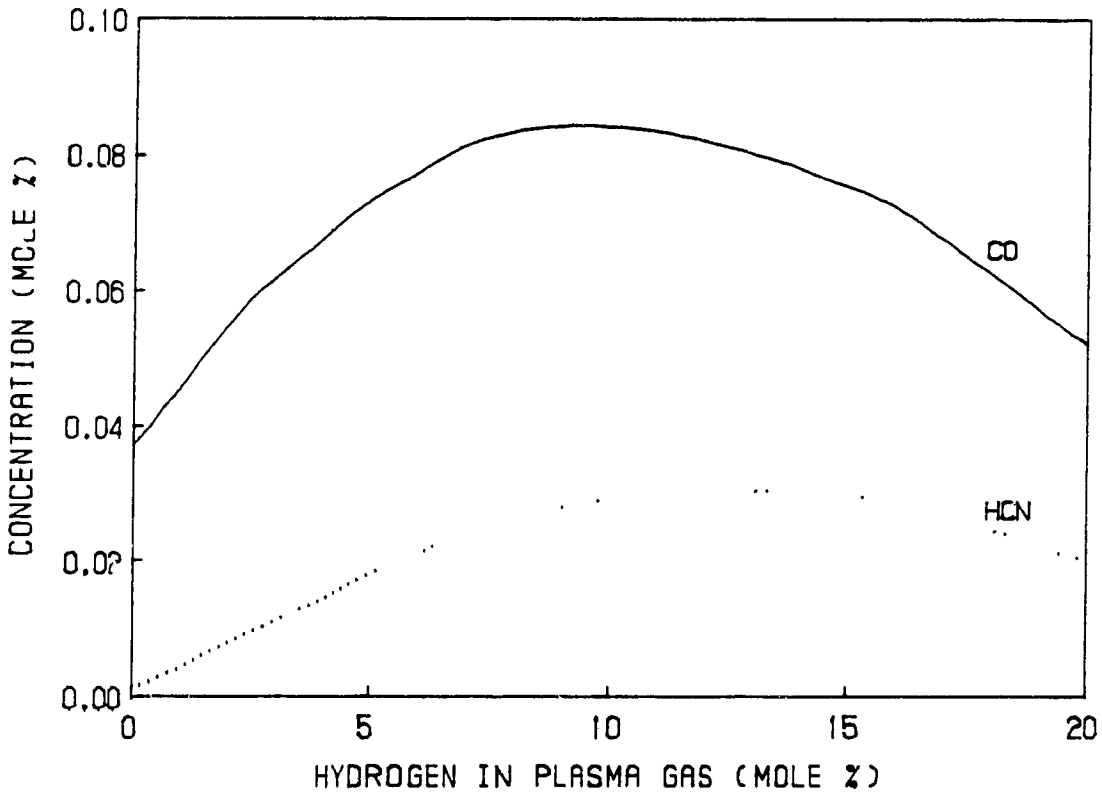

Figure 6.17

Variation of the Predicted Equilibrium Concentration of CO and HCN with Plasma Gas Composition. The temperature and the reaction stoichiometry vary as shown in Table 6.3.

conversion) was a strong function of heat transfer. Thus, one would expect CO and HCN to follow similar profiles to that of heat transfer (Figure 6.4), because higher rate of heat transfer would result in reacting more residue and, therefore, producing more CO and HCN.

Plasma temperature seemed to have different effects on the amount of CO and HCN present at equilibrium. The concentration of carbon monoxide increased almost linearly with increasing temperature as shown in Figure 6.16. This again is due to the increase in heat transfer with temperature resulting in the release of more oxygen into the gas phase. The decline in the concentration of HCN beyond 3500 K could either be due to its instability at high temperature or due to the decline in the amount of hydrogen in the gas phase, since more hydrogen would be ionized at high temperature. The decrease in hydrogen concentration at high temperature is evident in Figure 6.14.

6.6.4 Effect of Including Graphite as a Solid Phase

Solid carbon in the form of graphite was included in some calculations to determine the effect of considering solid phase on the equilibrium composition. It is more realistic to consider solid carbon especially at temperatures lower than the sublimation temperature of carbon (3800 K). However, for small residue conversion, as it is the case in this work, the effect of including solid carbon is expected to be

minimal. The thermodynamic calculations were based on the amount of residue that pyrolysed (less than 10%). Thus, the moles of residue entering the reaction are so small relative to those of argon and hydrogen that only a small amount is expected to remain unreacted (in the solid form). This is especially true for the temperature range studied in this work (greater than 2700).

The predicted yield of hydrocarbons as a function of plasma gas composition and plasma temperature is shown in Figures 6.18 and 6.19 for equilibrium calculations with and without graphite. The yield is again defined as the moles of carbon converted to gaseous hydrocarbons per mole of carbon reacted (Equation 6.2). At low temperatures (less than 3000 K), more solid carbon is present at equilibrium; therefore less carbon is converted to gaseous products. Consequently, the yield is lowered when graphite is included in the calculations as shown in Figure 6.18. Also, since increasing hydrogen concentration lowers temperature, the yield is lower at high hydrogen concentrations (greater than 15%) as shown in Figure 6.19.

6.6.5 Comparison with Experimental Results

The yield of hydrocarbon gaseous products (calculated and experimental) versus plasma gas composition and plasma temperature is shown in Figures 6.20 and 6.21 respectively. The thermodynamic calculations are plotted for both homogeneous (gas phase only) and heterogeneous (with graphite as a solid phase) system.

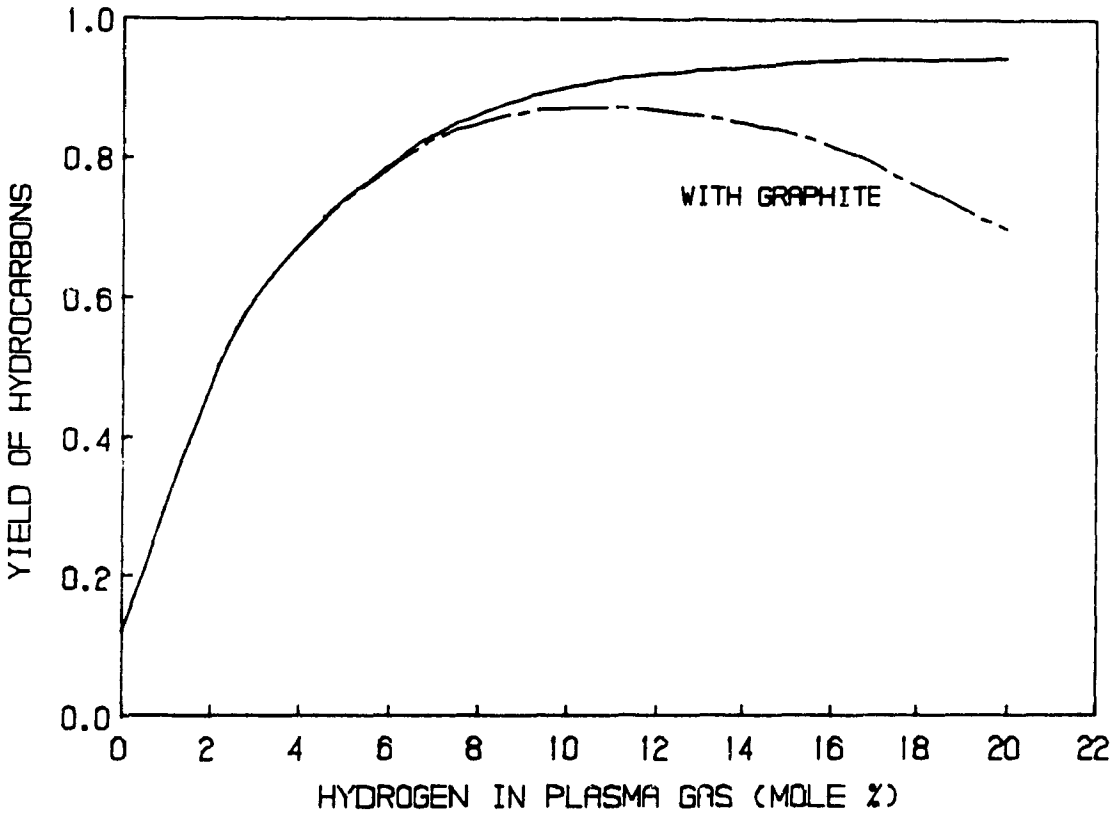

Figure 6.18

Predicted Yield of Hydrocarbons as a Function of Plasma Gas Composition. The temperature and the reaction stoichiometry vary as shown in Table 6.3.

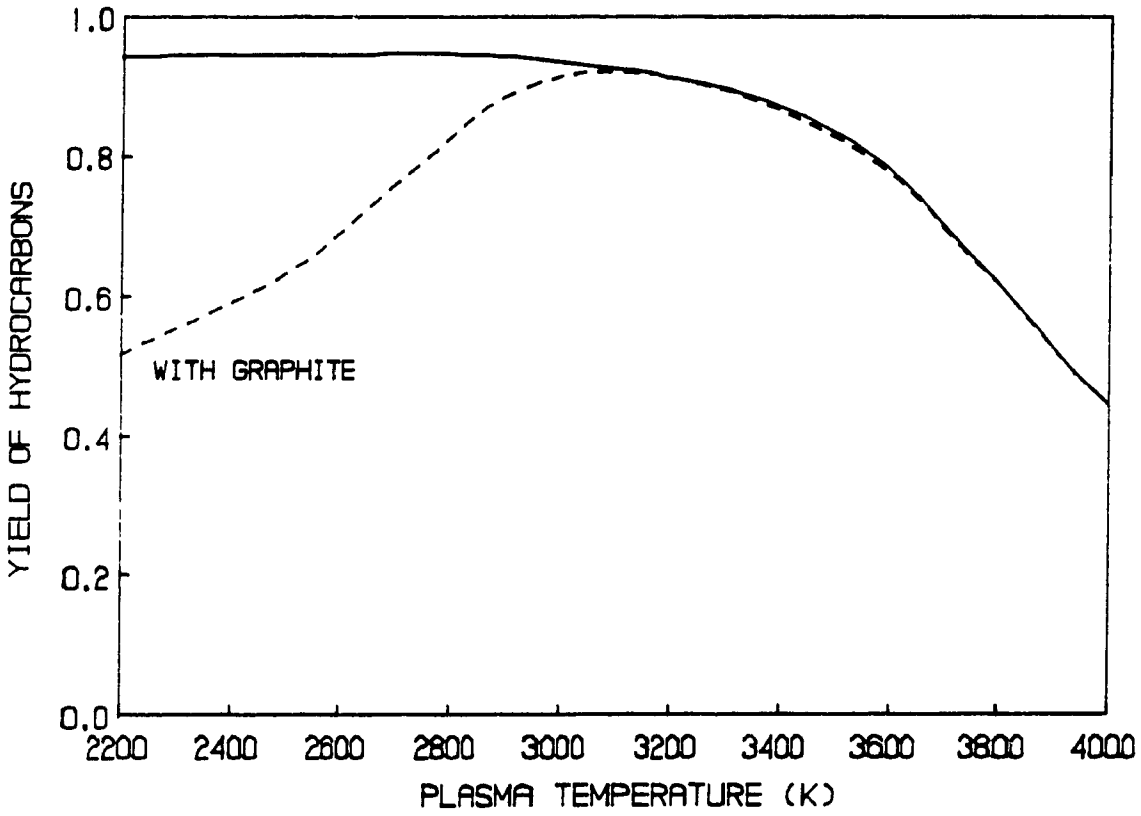

Figure 6.19

Predicted Yield of Hydrocarbons as a Function of Plasma Temperature. The reaction stoichiometry varies as shown in Table 6.2.

In thermodynamic analysis, it is assumed that carbon in the residue can either go to the gas phase or remain in the solid phase in the form of graphite. Graphite can only be present at low temperature (less than sublimation temperature of carbon 3800 K). In continuous pyrolysis, however, only part of the carbon goes into the gas phase or precipitates as soot; the rest is ejected as small droplets (particles). It is these ejected particles E_r that create the main difference between experimental results and thermodynamic calculations. Thus, since the rate of particle ejection was found to be strongly dependent on the rate of heat transfer (section 6.1), one would expect the disagreement between thermodynamic predictions and experimental results to be the greatest when the rate of heat transfer is the highest; that is at high plasma temperature and at moderate hydrogen concentration in the plasma gas. This is exactly the case as shown in Figures 6.20 and 6.21.

Thermodynamic calculations predicted considerable amounts of CO, HCN and H_2S at equilibrium. Experimentally, however, none of these gases was detected. Thermodynamics assumes that organic sulphur and oxygen are easily removed from the residue during the pyrolysis, while experimentally these elements are preserved in the unreacted portion of the residue especially at low conversion. Batch treatment of the CANMET residue by Dlugogorski (1989) showed that most of the organic sulphur and nitrogen were retained in the unconverted residue. Oxygen was released to form carbon monoxide. In continuous treatment, however, the short contact time between the residue and the plasma and the low pyrolysis temperature prevented the

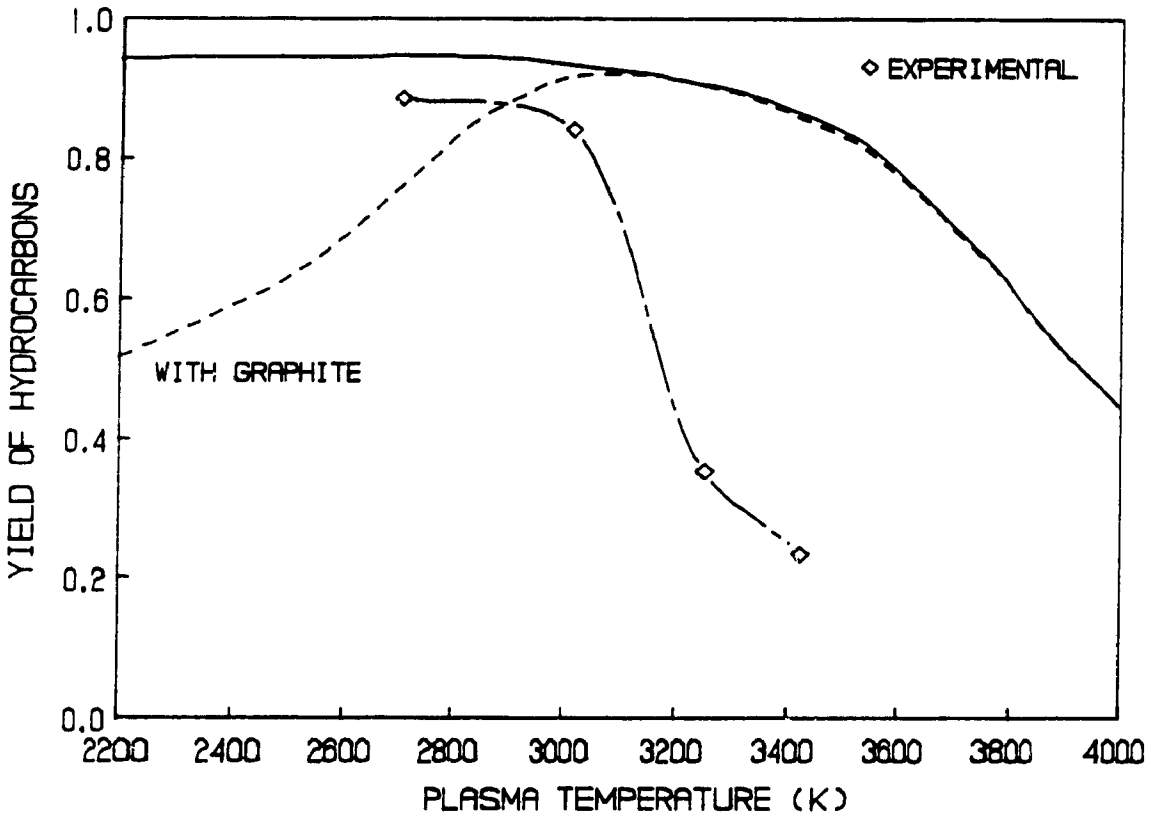

Figure 6.20

Predicted and Experimental Yield of hydrocarbons as a Function of Plasma Temperature. The reaction stoichiometry varies as shown in Table 6.2.

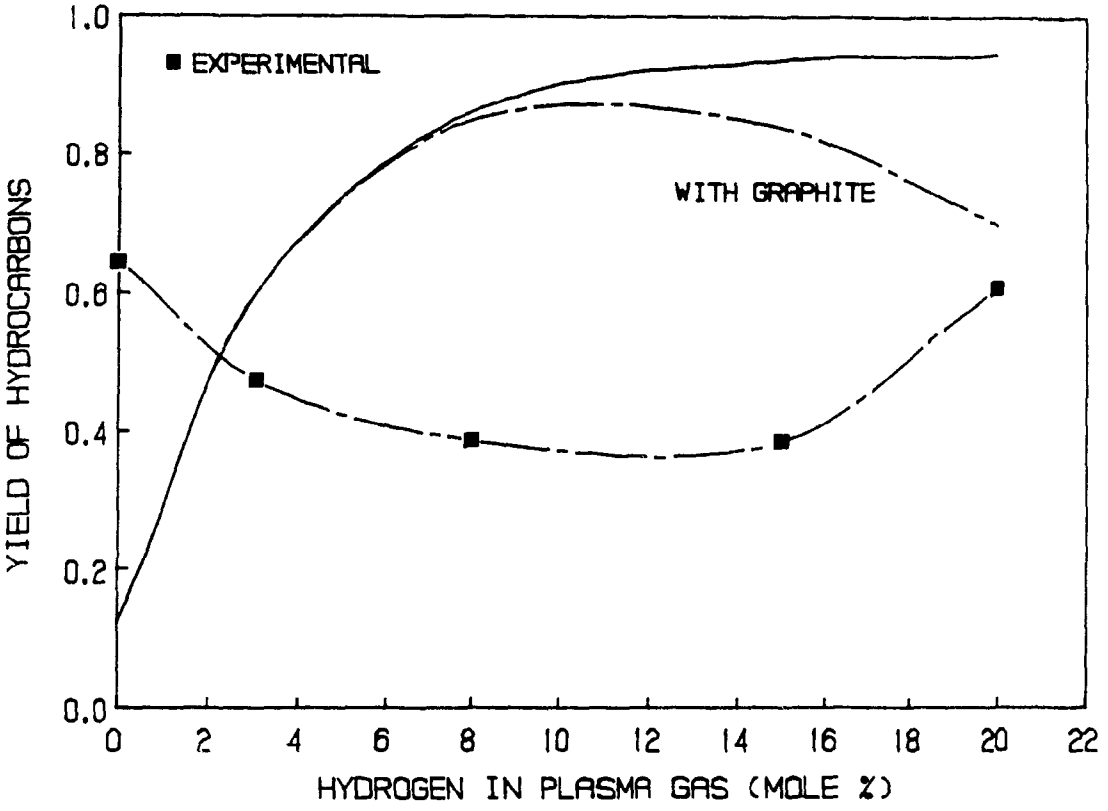

Figure 6.21

Predicted and Experimental Yield of Hydrocarbons as a Function of Plasma Gas Composition. The temperature and the reaction stoichiometry vary as shown in Table 6.3.

removal of oxygen and sulphur.

Although the disagreement between thermodynamic predictions and experimental results can be attributed to the variation in heat transfer and short reaction time as mentioned above, it is not clear whether plasma pyrolysis can reach thermodynamic equilibrium. Beiers et al (1988) argued that the reactions involved in plasma pyrolysis of hydrocarbons do not run into thermodynamic equilibrium. Thus, equilibrium composition may not be a valid prediction of the steady state product gas composition in continuous plasma pyrolysis.

6.7 COMPLETE CONVERSION

Continuous pyrolysis resulted in reacting only a small fraction of the residue (not more than 10 %); therefore it was not possible to determine whether complete pyrolysis was achievable. A few batch experiments were carried out to investigate the feasibility of completely reacting the organic part of the residue. A small molybdenum crucible (0.635 cm in internal diameter and 1 cm in depth) was used; the crucible was connected to a ceramic support through a thin stem (2 mm in diameter and 3 cm in length) to minimize heat loss. Small samples of residue (0.1 - 0.25 g) were treated at different plasma temperatures and plasma gas compositions for about 15 minutes. As soon as the plasma was started, the samples pyrolysed rapidly resulting in boiling off the volatiles in the residue. Part of the unreacted solids created a hollow dome

which covered the top of the crucible, while the rest stuck to the bottom and walls of the crucible. The part within the crucible appeared shiny when removed from the crucible. Analysis by X-ray diffraction of samples of this solid showed that it contained little carbon, and that the only recognizable compound it contained was iron sulphide (FeS).

The amount of residue reacted was found to depend on the operating conditions and the size of the sample. Conversion of the residue ranged from 47 to 71%. The highest conversion was achieved for a sample of 0.1 g at 8% hydrogen (plasma temperature of 3840 K). At these conditions, the crucible temperature was the highest at 2073 K as shown in Figure 6.22; the temperature was measured by a two wavelength digital pyrometer which was calibrated by the manufacturer between 1346 and 2773 K.

The 71% conversion achieved in these batch experiments was an improvement on the 50% achieved by Dlugogorski (1989). This is mainly due to the size of the crucible. The crucible used in this work was about eight times smaller than that used by Dlugogorski, and therefore had much less cooling by radiation. The smaller crucible gives higher conversion, because it has higher surface temperature. Thus, one could expect the organic part of the residue to pyrolyse completely if it were in direct contact with the plasma at high temperature.

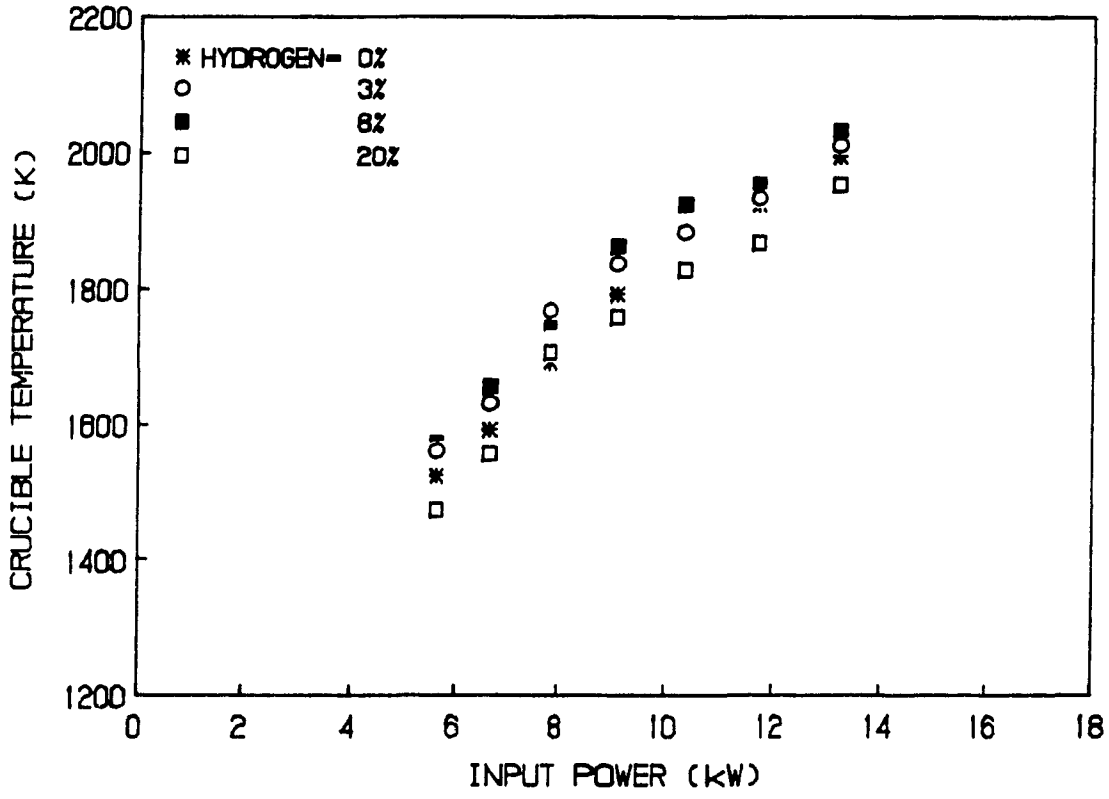

Figure 6.22

Variation of Crucible Temperature with Power Input.

- 7 -

CONCLUSIONS

The continuous pyrolysis of CANMET coprocessing residue in argon/hydrogen plasma was studied in the temperature range 2700 to 3670 K using an r.f. induction plasma torch. The residue was melted and continuously fed to a laboratory-scale reactor specially designed and built for the study. The residue flow rate was varied from 6 to 9 g/min. Hydrogen was injected into the argon plasma tailflame at molar concentrations of the total plasma gas ranging from 0 to 23%.

The effect of the various operating conditions on the residue pyrolysis was mainly dependent upon how much these conditions affected the rate of heat transfer. Increasing the plasma temperature increased the rate of heat transfer to the residue and, consequently, improved the pyrolysis. The rate of heat transfer reached a maximum at moderate hydrogen concentrations (10 to 15%) and so did the rate of pyrolysis. Also, because the residue flow rate, especially the range studied in this work, had negligible effect on heat transfer, the effect of the residue flow rate on residue pyrolysis was minimal.

The residue pyrolysis and the rate of formation of the gaseous products were strongly controlled by heat transfer. The formation of the gaseous products is believed to occur through the combination of three different steps: (1) the residue pyrolysis; this involves the breakdown of the residue resulting in the release of carbon and carbon radicals and the ejection of small residue droplets (or particles) into the gas phase. (2) homogeneous reaction; this is the reaction of carbon and carbon radicals with

hydrogen. (3) heterogenous reaction; this is the reaction of the ejected droplets with hydrogen while they are entrained in the gas. The contribution of this last step is believed to be small relative to that of the homogeneous reaction. The pyrolysis is the rate determining step and it is controlled by heat transfer.

A maximum of 10% of the treated residue pyrolysed with up to 90% conversion to gaseous hydrocarbons. The only gaseous products detected were acetylene, ethylene and methane. Acetylene was by far the major product, and, in agreement with thermodynamic predictions, its concentration in the product gas reached a maximum between 2800 and 3200 K. Other gases such as CO, HCN and H_2S were not detected despite thermodynamic predictions of considerable amounts of these gases. This was due to the low residue surface temperature (pyrolysis temperature). At such low temperature only, volatiles were removed from the residue; organic oxygen and sulphur were preserved in the unreacted residue.

Attempts were made to condense any liquid hydrocarbons, but no liquids were isolated. The complex aromatic structure of the CANMET residue and, probably, the high plasma temperature are believed to be the main reasons for the absence of liquid hydrocarbons.

Although soot was observed at the reactor outlets, the amount deposited in each single experiment was not sufficient for independent analysis; thus the deposition rate

could not be quantified or related to the various operating condition. Cumulative soot samples were collected and analyzed. The analysis showed that 28% of the carbon in the soot came from partially reacted residue droplets or particles ejected into the gas phase during the pyrolysis. Only 28% of these particles had reacted while entrained in the gas.

Elemental analysis of the unreacted residue, at the various operating conditions, showed that there was no change from the original residue. This indicated that at those conditions, the pyrolysis was uniform and that there was no preferential removal of carbon, hydrogen or nitrogen.

A few batch experiments were conducted to determine the feasibility of complete conversion of the organic part of the residue. The experiment were similar to those conducted by Dlugogorski (1989). The results showed that up to 71% of the treated residue reacted. This was an improvement on the 50% achieved by Dlugogorski. The use of a smaller crucible reduced cooling of the crucible by radiation resulting in higher crucible temperature and higher conversion. Thus, the organic part of the residue could pyrolyse completely if it were in direct contact with plasma at high temperature.

REFERENCES

Baronnet J. M., Lesinski J., Sauvage B., Vandensteendam C. and **Meillot E.,** Hydropyrolysis of Heavy Oils in H_2/CH_4 Arc Plasma, Eighth Int. Symp. Plasma Chem., Tokyo, 1987.

Baumann H., Bittner D., Beiers H. -G., Klein J. and **Jüntgen H.,** Pyrolysis of Coal in Hydrogen and Helium Plasmas, Fuel, Vol. 64, No. 8, 1988, PP. 1120 - 1123.

Beiers H. -G., Baumann H., Bittner D., Klein J., and **Jüntgen H.,** Pyrolysis of Some Gaseous and Liguid Hydrocarbons in Hydrogen Plasma, Fuel, Vol. 67, No. 7, 1988. PP. 1012 - 1016.

Biceroglu O., Clorination Kinetics of ZrO_2 in an R. F. Plasma Tailflame, Ph.D. Thesis, McGill University, 1978.

Bolouri S. and **Amouroux J.,** Acetylene Black Production in a Plasma Pilot Plant, Sixth Int. Conf. Plasma Chem., Montreal, 1983.

Dlugogorski B. Z., The Treatment of Vacuum Distilled Residue from the CANMET Process in Argon/Hydrogen Plasmas, M. Eng. Thesis, McGill University, 1989.

Fauchais P., Boulos M. and **Pfender E.,** Physical and Thermdynamic Properties of Thermal Plasma, Chapter 3 in "Plasma Technology in Metallurgical Processing", Ed. by Feinman J., Iron and Steel Society, Inc., 1987.

Gehrmann K. and **Schmidt H.,** Pyrolysis of Hydrocarbons Using a Hydrogen Plasma, Eighth World Congress, Moscow, 1971. PP. 378 - 388.

Hikita T., Takahashi I. and **Tsuru Y.,** Hydropyrolysis of Heavy Oils, Fuel, Vol. 68, No. 9, 1989, PP. 1140 - 1145.

JANAF Thermochemical Tables, National Bureau of Standards, Washington D. C., June 1971.

Kubanek G., Heavy Oil Processing in Steam and Hydrogen Plasmas, M. Eng. Thesis, McGill University, 1985.

Labort M., Talandier F. and **Moneuse M.,** Application des Torches á Plasma dans l'industrie, Rev. Gen. Elect., Vol. 90, No. 12, 1981, PP. 916 - 925.

McTaggart, "Plasma Chemistry in Electrical Discharges", Elserier Publishing Company, Amsterdam, 1967.

Mehmetoglu T., Characteristics of a Transferred-arc Plasma, Ph.D. Thesis, McGill University, 1980.

Menzies M. A., Silva A. E. and **Denis J. M.,** Hydrocracking without Catalysis Upgrades Heavy Oil, Chem. Eng., Vol. 88, No. 44, 1981, PP. 46 - 47.

Munz R. J., Decomposition of Molybdenum Disulphide in an Induction Plasma Tailflame, Ph.D. Thesis, McGill University, 1974.

Patterson P. A., Laser Doppler Anemometry in Transferred-arc Plasma, M. Eng., McGill University, 1983.

Pfender E., Boulos M., Fauchais P., Methods and Priciples of Plasma Generation, Chapter 4 in "Plasma Technology in Metallurgical Processing", Ed. by

Feinman J., Iron and Steel Society Inc., 1987.

Plooster M. N. and **Reed T. B.,** Carbon-Hydrogen-Acetylene Equilibrium at High Temperatures, J. Chem. Phys., Vol. 31, No. 1, 1959, PP. 66 - 72.

Rahimi P. M., Fouda S. A., Kelly J. F., Malhotra R. and **McMillen D. F.,** Characteristics of CANMET Coprocessing Distillate at Different Coal Concentrations, Fuel, Vol. 68, No. 4, 1989, PP. 422 - 429.

Sayegh N. N., Variable Property Flow and Heat Transfer to Single Spheres, Ph.D. Thesis, McGill University, 1977.

Schumacher M. M., Ed., "Heavy Oil and Tar Sands Recovery and Upgrading: International Technology", Noyes Data Corporation, Park Ridge, New Jersey, 1982.

Smith W. R. and **Missen R. W.,** "Chemical Reaction Equilibrium Analysis: Theory and Algorithms", John Wiley & Sons, New York, 1982.

Spangenberg H. -J., Formation and Decomposition of Acetylene in Thermal Plasma, Z. Chem., Vol. 21, No. 5, 1981, PP. 165 - 175.

Venugopalan M., Roychowdhury U. K., Chan K. and **Pool M. L.,** Plasma Chemistry of Fossil Fuels, in "Topics in Current Chemistry", Vol. 90, Plasma Chemistry II, Ed. by Veprek S. and Venugopalan M., Springer-Verlag, Berlin,1980, PP. 1 - 57.

White W. B., Johnson S. M. and **Dantzig G. B.,** Chemical Equilibrium in Complex Mixures, J. Chem. Phys., Vol. 28, No. 5, 1958, PP. 751 - 755.

APPENDICES

APPENDIX A

The following figures (Figure A.1 to A.8) contain calibration curves for the various gases used a to calibrate the gas partitioner. The gas partitioner was a Fisher Model 1200. It was running at 353 K using a combination of two columns in series (Propak N and Molecular Sieve 5 A). The carrier gas was a mixture of 8.5% hydrogen in helium, and its flow rate was set at 26 cm^3/min.

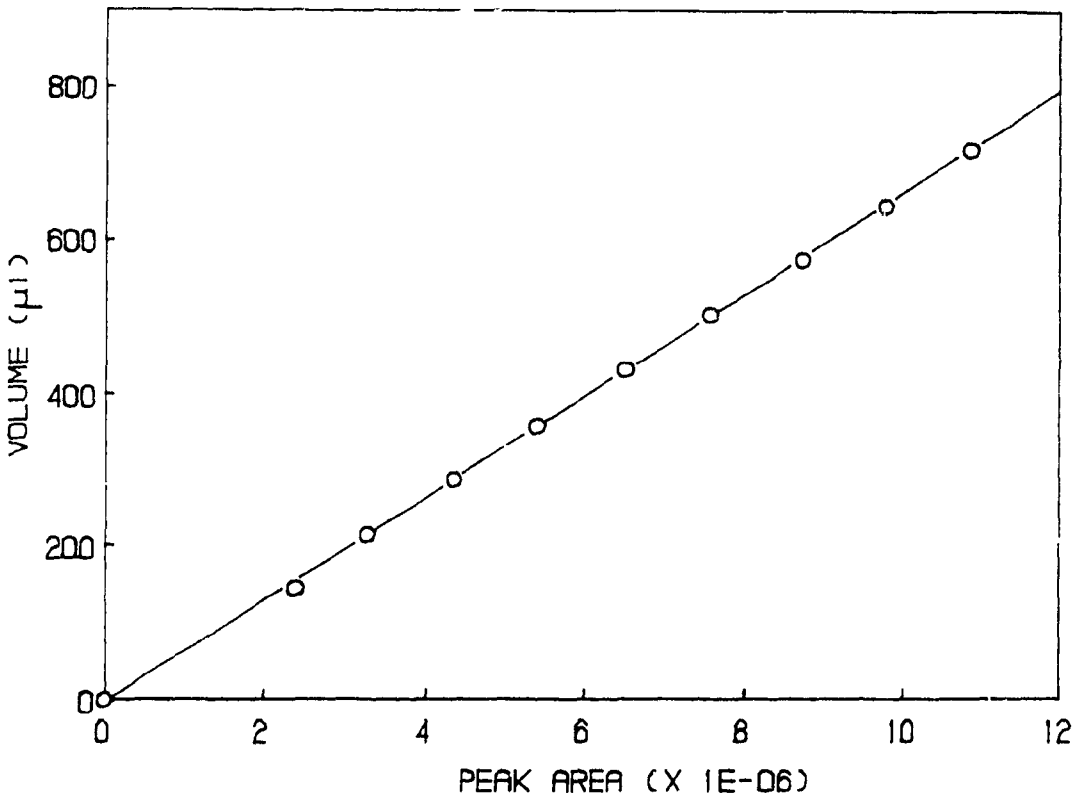

Figure A.1

Calibration for Argon.

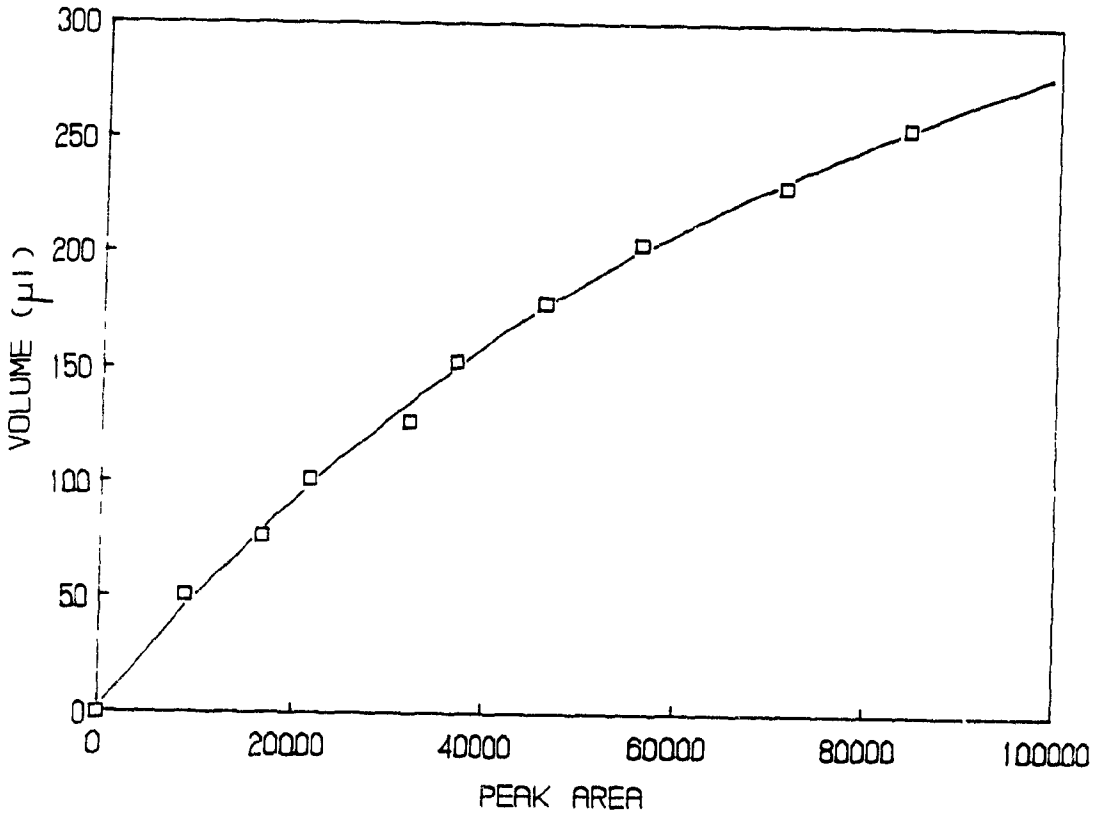

Figure A.2

Calibration for Hydrogen.

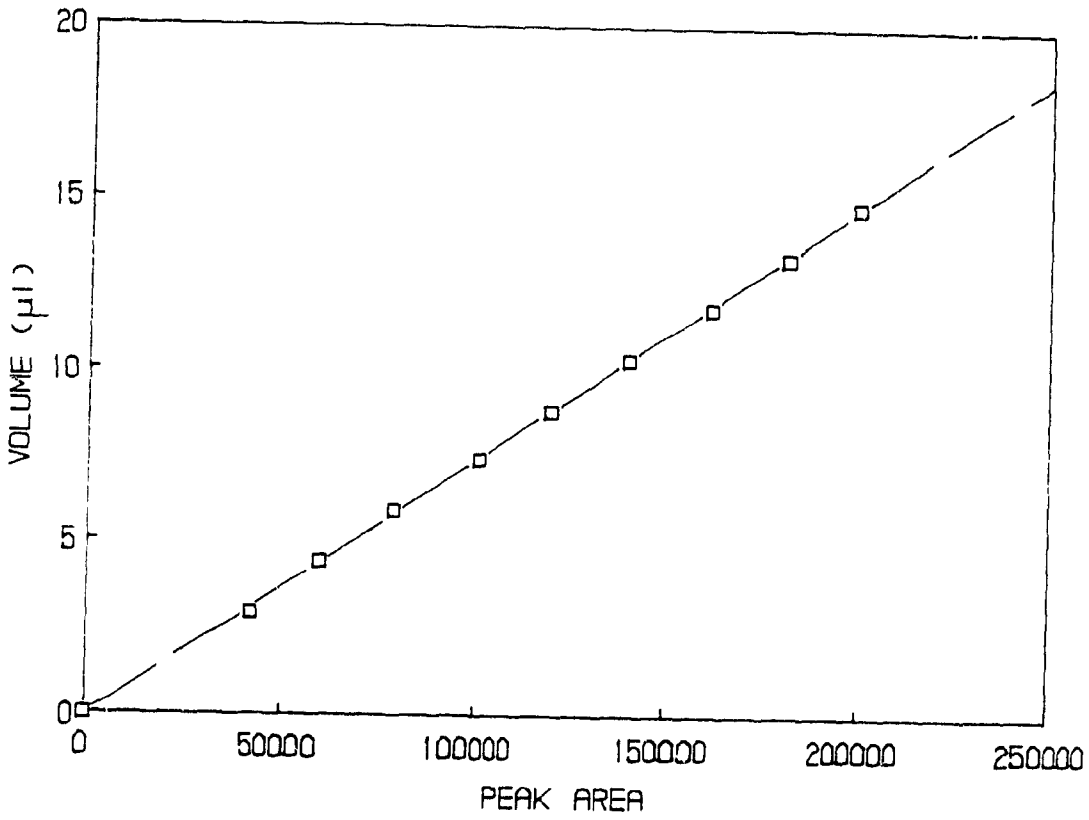

Figure A.3

Calibration for Acetylene.

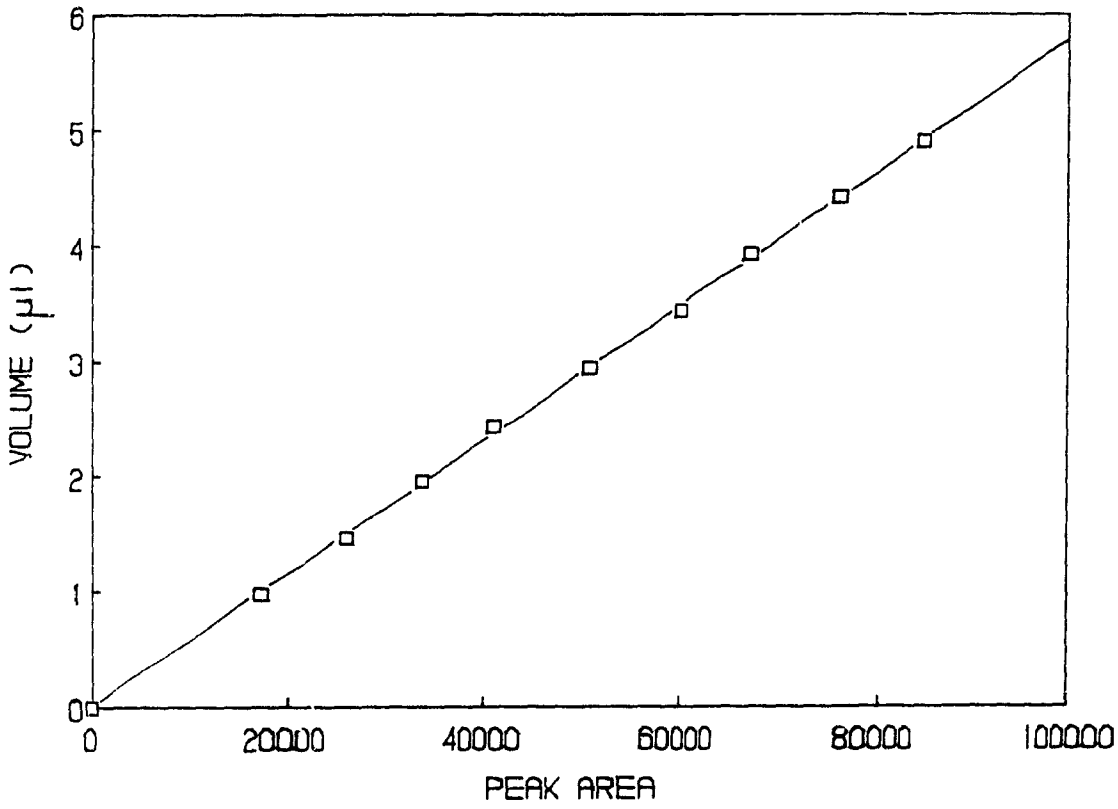

Figure A.4

Calibration for Ethylene.

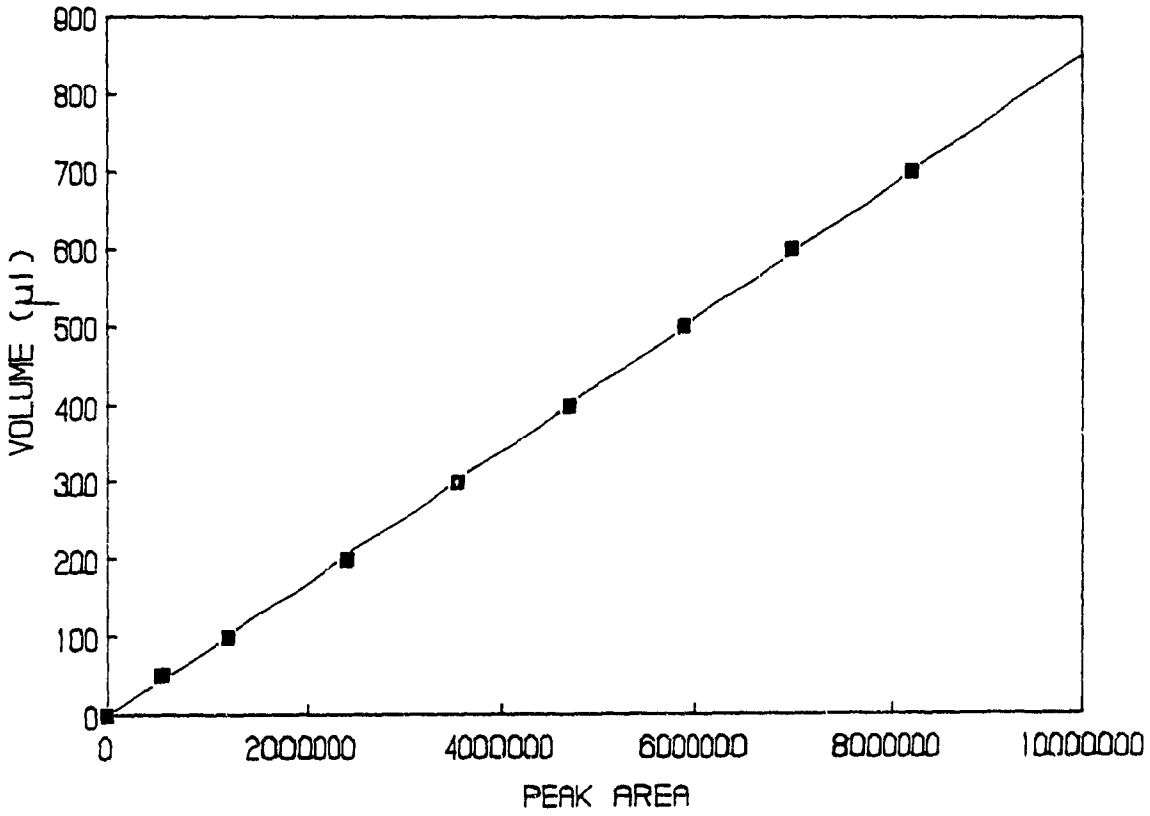

Figure A.5

Calibration for Methane.

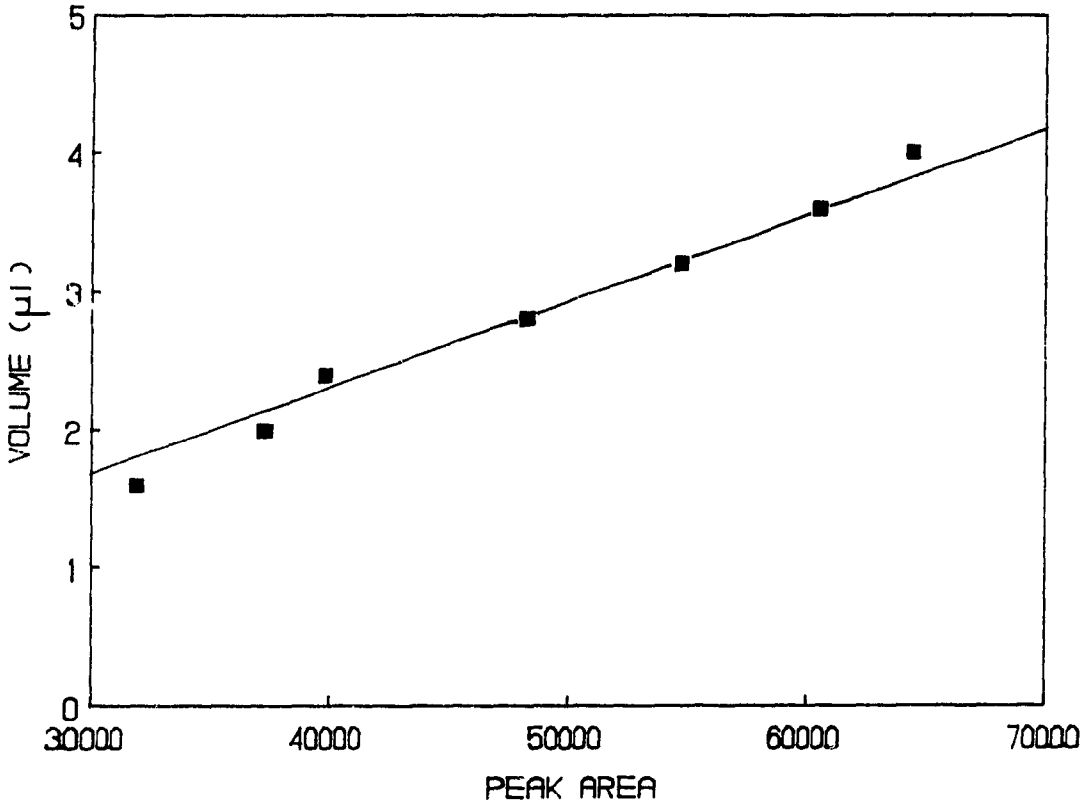

Figure A.6

Calibration for Nitrogen.

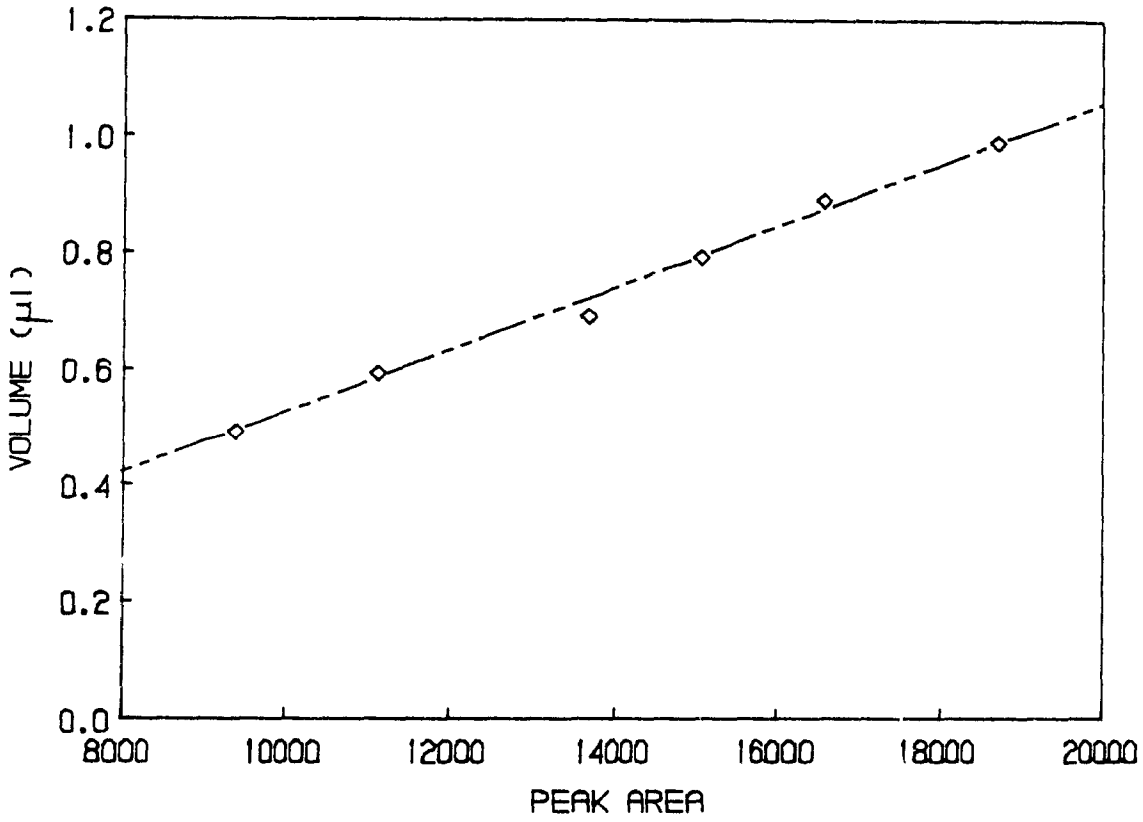

Figure A.7

Calibration for Carbon Dioxide.

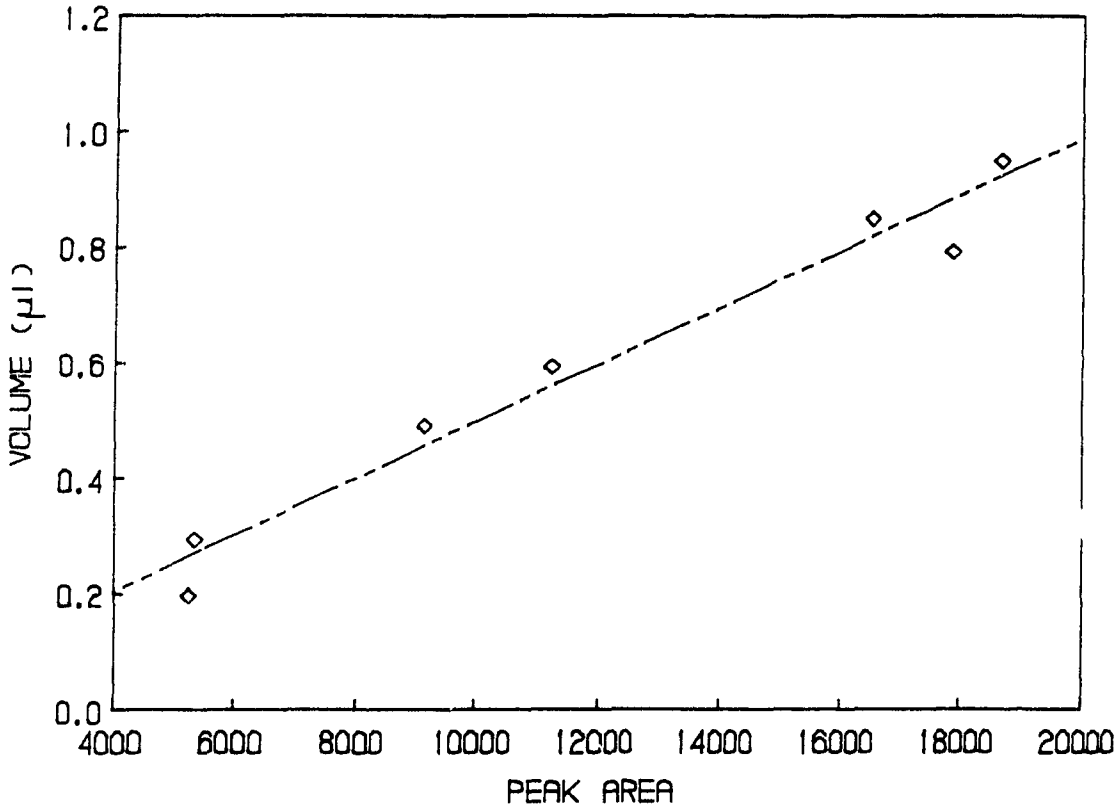

Figure A.8

Calibration for Carbon Monoxide.

APPENDIX B

Calculation of the Fraction of the Residue Solid Particles in the Soot. These calculations are based on the analyses given in Table 6.1.

Assume that the particles have the same composition as that of the CANMET residue.

Definitions:

M_S = total mass of the soot.

M_P = mass of particles in the soot.

M_C = mass of carbon black in the soot.

y_c = mass fraction of carbon in the soot (0.928)

y_h = mass fraction of hydrogen in the soot (0.0163)

x_c = mass fraction of carbon in the particles (depends on how much of these particles had reacted)

x_h = mass fraction of hydrogen in the particles (depends on how much of these particles had reacted)

As a first approximation, assume that the particles did not react while entrained in the gas phase (i.e. conversion = 0).

$$\therefore \quad x_c = 0.793, \quad x_b = 0.0633$$

Over all mass balance,

$$M_S = M_P + M_C$$

Carbon mass balance,

$$y_c M_S = M_S - M_P + x_c M_P$$

$$M_S (1 - y_c) = M_P (1 - x_c)$$

$$\therefore \quad M_P/M_S = (1 - y_c)/(1 - x_c)$$

$$= (1 - 0.928)/(1 - 0.793)$$

$$= 0.348 \quad \text{or } 34.8\%$$

Hydrogen mass balance,

$$y_b M_S = 0 + x_b M_P$$

$$\therefore \quad M_P/M_S = y_b/x_b = 0.0163/0.0633$$

$$= 0.258 \text{ or } 25.8\%$$

The disagreement between the carbon and hydrogen balance calculations indicates that the assumption of no reaction (conversion = 0) is not valid.

Thus, assume that the ejected particles react, while they are entrained in the gas phase, and that only carbon and hydrogen are removed from these particles at an equimolar ratio to form acetylene.

First assume that 10% of the particles had reacted (conversion = 10%).

For a basis of 100 g,

mass of carbon = 79.300 g (Table 6.1)

mass of hydrogen = 6.330 g

balance = 14.370 g

Amount reacted = 10 g (at a carbon-to-hydrogen molar ratio of 1 : 1 or mass ratio of 12 : 1.008)

$\therefore$ carbon reacted = 9.225 g

hydrogen reacted = 0.775 g

Amount left unreacted = 90 g

mass of carbon = 70.075 g

mass of hydrogen = 5.555 g

balance = 14.370 g

$\therefore$ $x_c = 0.7786$, and $x_h = 0.0617$

Carbon mass balance,

$$M_p/M_s = (1 - 0.928)/(1 - 0.7786)$$

$$= 0.325 \quad \text{or } 32.5\%$$

Hydrogen mass balance,

$$M_p/M_s = 0.0163/0.0617$$

$$= 0.264 \quad \text{or } 26.4\%$$

Both mass balance calculations seem to converge. Thus, one needs to assume higher conversion to get both calculations to give the same value for M_p/M_s. At a conversion of 28%, both carbon and hydrogen mass balance calculations give M_p/M_s = 0.282 or 28.2%. Thus, 28.2% of the soot comes from ejected particles; 28% of the particles react in the gas phase.

APPENDIX C

Heat Capacity at Constant Pressure for Carbon, Hydrogen, Oxygen, Sulphur and Nitrogen Containing Compounds in cal/deg.mole.

(Dlugogorski, 1989).

Table C.1

Values for A, B, C and D in Equation 6.3 for the Temperature Range 298-2000 K.

compound	A	B	C	D
C, carbon graphite	2.54496	3.76062	-1.40453	-1.06390
C, carbon monatomic	5.00382	-0.07271	-0.00466	0.03656
CH, methylidyne	5.77979	2.24097	0.51166	-0.41040
CH_2, methylene	6.03657	6.55366	-0.34108	-1.44282
CH_2O, formaldehyde	4.97794	12.99740	-0.14479	-3.26270
CH_3, methyl	5.35168	12.01646	0.06440	-2.90778
CH_4, methane	2.90432	18.46883	0.39229	-4.36814
CN, cyano	6.04789	2.33267	0.22558	-0.44529
CN_2, CNN radical	9.87687	4.08269	-0.81449	-0.97075
CN_2, NCN radical	11.67918	3.38549	-1.89493	-0.96091
CO, carbon monoxide	5.76104	2.78658	0.38372	-0.67723
CO_2, carbon dioxide	8.78884	5.74042	-1.36243	-1.47664
COS, carbon oxide sulfide	10.50338	4.33886	-1.60994	-1.11135
CS, carbon monosulphide	7.02220	2.07721	-0.43943	-0.57783
CS_2, carbon disulfide	11.84482	3.19038	-1.66966	-0.88516
C_2, carbon diatomic	7.49641	0.85508	2.31922	0.00175
C_2H, CCH radical	8.52467	4.62995	-0.85969	-0.92629
C_2H_2, acetylene	10.42363	7.57657	-1.79241	-1.51452
C_2H_4, ethylene	7.11547	20.31574	-2.30270	-4.90956
C_2H_4O, ethylene oxide	9.34893	24.44838	-4.28081	-5.11900
C_2N, CNC radical	12.21787	2.91500	-1.88692	-0.84509
C_2N_2, cyanogen	13.36476	6.63002	-1.46898	-1.76013
C_2O, CCO radical	9.63186	5.67788	-0.82297	-1.48283
C_3, carbon trimeric	9.32810	5.27370	-1.26642	-1.39731
C_3O_2, carbon suboxide	16.23343	9.82456	-2.65266	-2.56652
C_4, carbon tetratomic	13.01649	7.36745	-2.02986	-1.94026
C_4N_2, tetracarbon dinitr	20.61424	10.98724	-2.80941	-2.81242
C_5, carbon pentatomic	16.70489	9.46119	-2.79329	-2.48320
H, hydrogen monatomic	4.96800	0.00000	0.00000	0.00000
HCN, hydrogen cyanide	7.93470	5.26679	-0.74630	-1.13890
HCO, formyl	6.54668	6.09550	0.01045	-1.47080
HNCO, isocyanic acid	10.65539	7.32941	-1.77578	-1.73193
HNO, nitroxyl hydride	6.81547	6.14069	-0.23250	-1.53408
HNO_2, cis-nitrous acid	11.43758	6.97504	-2.14890	-1.71240
HNO_2, trans-nitrous acid	19.31528	0.15793	-40.00383	-0.01266
HNO_3, nitric acid	14.05816	10.54997	-3.83503	-2.73746
HS, sulfur monohydride	6.40026	1.62150	0.83593	-0.23662
H_2, hydrogen	6.75908	0.22469	0.05311	0.25860
H_2O, water	6.15630	4.29092	0.58747	-0.62740
H_2S, hydrogen sulfide	5.81754	6.50373	0.48434	-1.45415
H_2SO_4, sulfuric acid	22.71293	12.51363	-6.24166	-3.10009
N_2, nitrogen monatomic	4.96941	-0.00261	-0.00069	0.00116
NH, imidogen	5.99408	1.65883	0.45748	-0.20535
NH_2, amidogen	5.72274	5.48065	0.69097	-1.08542
NH_3, ammonia	5.39016	10.20414	0.23566	-2.15439
NO, nitric oxide	5.94351	2.84355	0.35146	-0.73089

NO_2, nitrogen dioxide	8.51564	5.51761	-1.10667	-1.53917
NO_3^2, nitrogen trioxide	14.14342	6.27127	-4.21195	-1.82795
N_2, nitrogen diatomic	5.72016	2.64661	0.45389	-0.61022
N_2H_2, cis-diimide	6.36744	11.14704	-0.68535	-2.70303
$N_2H_4^2$, hydrazine	11.56806	15.12384	-3.29336	-3.40295
N_2O, dinitrogen monoxide	9.27316	5.32439	-1.37194	-1.41107
$N_2O_3^2$, dinitrogen trioxid	16.40950	8.47325	-2.78987	-2.33895
$N_2O_4^2$, dinitrogen tetroxi	20.19922	11.88457	-4.54546	-3.32081
$N_2O_5^2$, dinitrogen pentoxi	28.45555	8.39177	-7.00075	-2.50485
O^2, oxygen monatomic	5.02434	-0.06487	0.20599	0.01992
OH, hydroxyl	6.30934	1.00461	0.48627	-0.00133
O_2, oxygen diatomic	6.49137	2.39112	-0.13951	-0.57458
O_3^2, ozone	10.69062	3.58975	-2.09353	-0.99039
S^3, sulfur monatomic	5.71094	-0.85477	0.16813	0.27386
SN, monosulfur mononitri	7.28675	1.81844	-0.18536	-0.50275
SO, sulfur monoxide	7.37899	1.74161	-0.59413	-0.48595
SO_2, sulfur dioxide	9.97309	4.31686	-1.49269	-1.18919
SO_3^2, sulfur trioxide	13.62389	6.61075	-3.02835	-1.88537
S_2, sulfur diatomic	8.44106	0.62904	-0.76971	-0.16798
S_2O, disulfur monoxide	11.81364	2.28260	-1.71408	-0.66292
S_8^2, sulfur octatomic	42.76133	1.10011	-5.14489	-0.33032

Table C.2

Values for A, B, C and D in Equation 6.3 for the Temperature Range 2000-6000 K.

compound	A	B	C	D
C, carbon graphite	6.09011	-0.04583	-8.94461	0.02267
C, carbon monatomic	3.98941	0.46515	9.14459	-0.03527
CH, methylidyne	8.70919	0.19034	-17.88466	-0.00540
CH_2, methylene	14.27550	0.17934	-47.16951	-0.01444
CH_2O, formaldehyde	19.34893	0.15023	-60.49549	-0.01215
CH_3, methyl	19.26657	0.17218	-65.28157	-0.01381
CH_4, methane	24.64087	0.34110	-106.63616	-0.02752
CN, cyano	5.84451	1.97479	-4.20185	-0.18633
CN_2, CNN radical	14.66115	0.06940	-24.01149	-0.00560
CN_2, NCN radical	14.88128	0.00647	-10.02070	-0.00052
CO, carbon monoxide	8.86151	0.05742	-12.55877	0.00007
CO_2, carbon dioxide	15.03500	0.00014	-27.21928	0.01553
COS, carbon oxide sulfide	14.83685	0.17642	-16.61336	-0.00152
CS, carbon monosulphide	8.93191	0.05183	-5.22287	-0.00027
CS_2, carbon disulfide	14.87712	0.04300	-9.90428	-0.00064
C_2, carbon diatomic	8.56815	0.66540	-17.36162	-0.05511
C_2H, CCH radical	12.10897	1.67896	-29.42955	-0.16577
C_2H_2, acetylene	19.93691	0.58435	-61.17033	-0.02116
C_2H_2, ethylene	30.52274	0.36322	-114.09419	-0.02926
C_2H_4O, ethylene oxide	36.49157	0.36133	-123.68802	-0.02911
C_2N, CNC radical	15.17406	-0.12642	-11.60619	0.01622
C_2N_2, cyanogen	20.66531	0.05771	-30.87875	-0.00466
C_2O, CCO radical	16.98919	-0.38215	-45.79277	0.02089
C_3, carbon trimeric	14.79633	0.03141	-20.15039	-0.00256
C_3O_2, carbon suboxide	26.60451	0.06439	-40.26314	-0.00523
C_4, carbon tetratomic	20.70796	0.04637	-28.95976	-0.00382
C_4N_2, tetracarbon dinitr	32.58233	0.04739	-49.76798	-0.00285
C_5, carbon pentatomic	26.61959	0.06134	-37.76912	-0.00507
H, hydrogen monatomic	4.96800	0.00000	0.00000	0.00000
HCN, hydrogen cyanide	14.15677	0.38269	-34.71807	-0.03336
HCO, formyl	13.57863	0.09456	-32.81741	-0.00759
HNCO, isocyanic acid	19.27043	0.17113	-45.64356	-0.01375
HNO, nitroxyl hydride	13.64005	0.07792	-29.45828	-0.00633
HNO_2, cis-nitrous acid	19.31528	0.15793	-40.00383	-0.01266
HNO_2, trans-nitrous acid	11.43758	5.97504	-2.14890	-1.71240
HNO_3, nitric acid	25.27205	0.15965	-49.63293	-0.01282
HS, sulfur monohydride	8.86766	0.11253	-16.78771	-0.00235
H_2, hydrogen	7.66257	0.50969	-16.79177	-0.01587
H_2O, water	12.80011	0.45985	-56.52941	-0.02761
H_2S, hydrogen sulfide	13.50928	0.27591	-38.67037	-0.00931
H_2SO_4, sulfuric acid	36.72917	0.29051	-73.74549	-0.02326
N, nitrogen monatomic	5.11943	-0.27586	4.91080	0.07349
NH, imidogen	8.57852	0.22062	-20.49718	-0.00784
NH_2, amidogen	13.19963	0.20240	-47.57982	-0.01628
NH_3, ammonia	16.79314	1.04894	-64.57130	-0.02605
NO, nitric oxide	8.88638	0.06408	-10.02333	-0.00137

NO_2, nitrogen dioxide	13.86265	0.01403	-15.87568	-0.00116
NO_3, nitrogen trioxide	19.85359	0.00507	-16.78257	-0.00038
N_2, nitrogen diatomic	8.92185	0.02282	-15.42824	0.00405
N_2H_2, cis-diimide	19.16572	0.20087	-61.68049	-0.01613
N_2H_4, hydrazine	30.20596	0.45211	-109.04638	-0.03634
N_2O, dinitrogen monoxide	14.79709	0.03066	-20.52950	-0.00246
N_2O_3, dinitrogen trioxid	24.75281	0.02496	-27.28276	-0.00199
N_2O_4, dinitrogen tetroxi	31.69017	0.03052	-36.11062	-0.00247
N_2O_5, dinitrogen pentoxi	35.68256	0.03372	-17.84406	-0.00318
O, oxygen monatomic	4.55535	0.11746	7.59649	0.00134
OH, hydroxyl	8.41590	0.24089	-22.86332	-0.01197
O_2, oxygen diatomic	7.70033	0.82585	-2.71610	-0.06624
O_3, ozone	13.89579	0.13021	-9.31222	-0.00034
S, sulfur monatomic	4.12424	-0.47771	6.60917	-0.04133
SN, monosulfur mononitri	8.95393	0.05582	-4.73623	0.00032
SO, sulfur monoxide	8.93888	0.05781	-4.26886	-0.00002
SO_2, sulfur dioxide	13.88515	0.15589	-11.12073	-0.00059
SO_3, sulfur trioxide	19.83844	0.00957	-18.47999	-0.00076
S_2, sulfur diatomic	8.94253	0.06358	-1.77747	-0.00001
S_2O, disulfur monoxide	13.90231	0.00244	-6.39696	-0.00019
S_8, sulfur octatomic	43.71730	0.00068	-6.85870	-0.00005